Redox Biology 52 (2022) 102320

Contents lists available at ScienceDirect

Redox Biology

journal homepage: www.elsevier.com/locate/redox

Increased fatty acid metabolism attenuates cardiac resistance to β-adrenoceptor activation via mitochondrial reactive oxygen species: A potential mechanism of hypoglycemia-induced myocardial injury in diabetes

Lishan Huang [a,1], Zhou Chen [b,1], Ruiyu Chen [b], Lu Lin [a], Lingjia Ren [a], Meilian Zhang [c], Libin Liu [a,*]

[a] Department of Endocrinology, Fujian Medical University Union Hospital, Fuzhou, China
[b] School of Pharmacy, Fujian Medical University, Fuzhou, China
[c] Department of Ultrasound, Fujian Province Hospital for Women and Children, Fuzhou, China

ARTICLE INFO

Keywords:
Hypoglycemia
Diabetes
Lipid metabolism
β-adrenoceptor
Mitochondrial reactive oxygen species

ABSTRACT

The mechanism of severe hypoglycemia (SH)-induced cardiovascular disease in diabetes remains unknown. Our previous study found that SH inhibits cardiac function and lipid metabolism in diabetic mice. Conversely, in nondiabetic mice, SH does not induce cardiac dysfunction but promotes cardiac lipid metabolism. This study aims to clarify the effect of increased fatty acid metabolism on the resistance of cardiomyocytes to β-adrenoceptor activation during hypoglycemia in diabetes. Results revealed that cardiomyocytes with enhanced lipid metabolism were more vulnerable to damage due to β-adrenoceptor activation, which presented as decreased cell viability, disorder of mitochondrial structure, dissipation of mitochondrial membrane potential, dysfunction of mitochondrial oxidative phosphorylation, nonapoptotic damage, and accumulation of ROS and calcium from mitochondria to cytoplasm, all of which were partially reversed by mitochondrial antioxidant Mito-TEMPO. The SH-induced cardiac dysfunction, and reduction of myocardial energy metabolism in diabetic mice were rescued by Mito-TEMPO. Our findings indicate that high fatty acid metabolism crippled cardiac resistance to β-adrenoceptor hyperactivation, with mitochondrial ROS playing a pivotal role in this process. Reducing mitochondrial ROS in diabetes could disrupt this synergistic effect and prevent poor cardiac outcomes caused by SH.

1. Introduction

Hypoglycemia is considered the strongest predictor of adverse cardiovascular outcomes in patients with diabetes [1]. Hypoglycemia tends to trigger such events in patients with diabetes with other preexisting cardiovascular risk factors [2], suggesting the potential existence of synergistic factors in hypoglycemia and diabetes, which jointly determine the fate of cardiovascular outcomes. Our previous study discovered that severe hypoglycemia (SH)-afflicted diabetic mice showed inhibited lipid metabolism and aggravated cardiac injuries, whereas nondiabetic SH-inflicted mice did not show cardiac dysfunction but showed enhanced cardiac lipid metabolism [3].

Activation of the sympathoadrenal system is considered a key driver of adverse cardiovascular events following SH [2,4]. Sympathetic excitation is known to activate β-adrenergic receptors in the heart, resulting in fatal arrhythmias and sudden death in diabetic rats due to SH [5]. The isoproterenol (ISO) β-adrenergic agonist significantly inhibited myocardial lipid metabolism in a dose-dependent manner [6]. Therefore, a crucial role of β-adrenoceptor activation was speculated to aggravate cardiac function and lipid metabolism in diabetic mice. However, the similarity in the activity of sympathetic nerves between diabetics and non-diabetics during hypoglycemia [7,8] cannot explain the preserved cardiac function and lipid metabolism in nondiabetic mice despite SH. Thus, the underlying basis between individuals with and without diabetes might be vital for explaining the differences in

Abbreviations: TMRE, tetramethylrhodamine ethyl ester.

* Corresponding author. Department of Endocrinology, Fujian Medical University Union Hospital, Fuzhou, 350001, Fujian, China.
E-mail address: Libinliu@fjmu.edu.cn (L. Liu).

[1] These authors contributed equally to this work and share the first authorship.

https://doi.org/10.1016/j.redox.2022.102320
Received 3 April 2022; Accepted 18 April 2022
Available online 21 April 2022

Abbreviations:

AIF	apoptosis-inducing factor
AR	aspect ratio
ATP	adenosine triphosphate
BCA	bicinchoninic acid
BSA	bovine serum albumin
CCK-8	cell counting kit-8
CD36	cluster of differentiation 36
COX I	complex I
COX IV	complex IV
CPT-1	carnitine palmityl transferase 1
cTnI	cardiac troponin I
cyt-c	cytochrome C
DFO	deferoxamine mesylate
DH	diabetic mice experiencing hypoglycemia
DHT	diabetic mice pretreated with Mito-TEMPO experiencing hypoglycemia
DM	diabetes mellitus
EDV	end-diastolic volume index
EF	ejection fraction
ELISA	Enzyme-linked immunosorbent assay
ESV	end-systolic volume index
FACS	fatty acyl coenzyme A synthetases
FATP-1	fatty acid transporter 1
Fer-1	ferrostatin-1
FF	form factor
FI	fluorescence intensity
FS	fractional shortening
GLUT4	glucose transporter 4
HBSS	Hanks' balanced salt solution
i.p.	intraperitoneal
ISO	isoproterenol
IVSd	interventricular septal thickness at diastole
IVSs	interventricular septal thickness in systole
LVIDd	left ventricular internal dimension at diastole
LVIDs	left ventricular internal dimension at systole
LVPWd	left ventricular posterior wall thickness in diastole
LVPWs	left ventricular posterior wall thickness in systole
LV Mass	left ventricular mass
MACD	medium-chain acyl-CoA dehydrogenase
mPTP	mitochondrial permeability transition pore
MT	Mito-TEMPO
mtROS	mitochondrial reactive oxygen species
OCR	oxygen consumption rate
OXPHOS	oxidative phosphorylation
PA	palmitic acid
PBS	phosphate-buffered saline
PI	propidium iodide
PVDF	polyvinylidene difluoride
ROS	reactive oxygen species
SH	severe hypoglycemia
STZ	streptozotocin
SV	stroke volume

cardiovascular outcomes in the context of SH.

The heart is an organ that depends almost exclusively on lipid metabolism [9]. An increase in free fatty acid levels is the key regulator signaling the heart to further enhance lipid metabolism and inhibit insulin-dependent uptake of glucose in diabetes [10]. Short-term exposure to a high concentration of palmitic acids could effectively activate mitochondrial respiration of cardiomyocytes with increased mitochondrial polarization and adenosine triphosphate (ATP) synthesis [11]. Meanwhile, β-adrenoceptor activation stimulates the heart to increase the force of contraction and rate of conduction, resulting in an escalating demand for energy supply [12]. However, although the diabetic heart tends to increase lipid metabolism in early stages, the efficiency of energy production by the mitochondria is decreased [13]. We speculated that high fatty acid metabolism in diabetes may induce more cardiac susceptibility to damage following β -receptor activation.

Mitochondria are considered as the major reactive oxygen species (ROS)-producing organelles, and ROS production increases following enhancement of mitochondrial oxidative phosphorylation in the context of diabetes [14]. Overactivation of β-adrenoceptor-induced damage and the death of cardiomyocytes are closely associated with ROS [15]. SH is known to accelerate the production of ROS in both nondiabetic and diabetic hearts [3]. Accordingly, it was hypothesized that mitochondrial ROS is the core factor mediating the synergistic effect between high fatty acid metabolism and β-adrenoceptor activation, leading to myocardial injury and energy metabolism disorders.

Hence, this study aimed to investigate whether increased fatty acid metabolism attenuates cardiac resistance to β-adrenoceptor activation via mitochondrial ROS (mtROS) to elucidate a potential mechanism and therapeutic target to prevent hypoglycemia-induced myocardial injury in diabetes.

2. Methods

2.1. Cell culture and intervention

The H9c2 rat cardiomyocyte cell line was purchased from Boleolin Biological Technology Co. Ltd (Fuzhou, Fujian, China). H9c2 cells were cultured in low-glucose DMEM (Cat.10567014; Gibco, NY, USA) containing 10% (v/v) fetal bovine serum (Cat.S712-012S; Lonsera, Shanghai, China), and 1% (v/v) penicillin and streptomycin (Cat.C0222; Beyotime, Shanghai, China) at 37 °C and 5% CO_2. When the cell density reached 80–90%, 500 μM palmitic acid (PA; P5585; Sigma-Aldrich, MO, USA)-conjugated 0.5% fatty acid free bovine serum albumin (BSA) (Cat.36104ES25; YEASEN; Shanghai, China) was added to the cell culture medium to mimic a high fatty acid environment [11,16]. After pretreatment, the medium containing isoproterenol was replaced, followed by another treatment. The Mito-TEMPO (MT) mitochondrial antioxidant (SML0737; Sigma-Aldrich) was added to cells cultured in a high concentration of fatty acids. Ferrostatin-1 (Fer-1; HY-100579; MedChenExpress, Shanghai, China) and deferoxamine mesylate (DFO; HY-B0988; MedChenExpress) were added during the ISO intervention.

2.2. Experimental animals and treatment

Male C57BL/6 J mice (20–25 g) were purchased from Vital River Laboratory Animal Technology (Beijing, China) and randomly divided in three groups: diabetic mice (DM), diabetic mice afflicted with SH (DH), and diabetic mice pretreated with MT suffering SH (DHT). Diabetes was induced in mice via a single intraperitoneal (i.p.) injection of 150 mg/kg streptozotocin (STZ; S0130; Sigma-Aldrich). On day 3 post-injection, a blood glucose level >16.7 mmol/L with symptoms of polyuria, polydipsia, polyphagia, and emaciation indicated the successful induction of diabetes. After fasting overnight, DH and DHT mice received an i.p. injection of regular insulin (15 mU/g; Wanbang, Jiangsu, China), to sustain a tail vein glucose level of <2.0 mmol/L for 90 min [3]. DHT mice were treated with 0.7 mg/kg/d MT (SML0737;

Sigma-Aldrich) twice before induction of SH [17]. Finally, one mouse in the DH group died and was excluded. Cardiac function was monitored, and samples were collected at 24 h after SH [3]. All animal experiments complied with the ARRIVE guidelines and carried out in accordance with the National Research Council's Guide for the Care and Use of Laboratory Animals.

3. Method details

3.1. Cell viability

After treatment, cells were washed with phosphate-buffered saline (PBS) and incubated in a culture medium containing 10% cell counting kit-8 (CCK-8) (Cat.BS350B; Biosharp, Hefei, China). After incubation at 37 °C for 1.5 h in the dark, the absorbance was measured at 450 nm using a spectrophotometer (MultiskanGO; Thermo Fisher Scientific, WA, USA).

3.2. Mitochondrial staining

After treatment, cells were washed using preheated Hanks' balanced salt solution (HBSS) buffer (Cat.C0219; Beyotime). A labeling solution containing 0.1 μM MitoTracker Red CMXRos (Cat.I35103; Thermo Fisher Scientific) was added to the cells and incubated at 37 °C away from light for 15 min. After washing with preheated HBSS buffer, cells were soaked in warm buffer and observed under a laser scanning confocal microscope (SP5; Leica, Frankfurt, Germany). There are two main quantitative indices of mitochondrial morphology, the aspect ratio (AR) and the form factor (FF), which were calculated using the Image Pro Plus 6.0 software (Media Cybernetics; MD, USA).

The FF value was calculated using the formula "$4 \times \pi \times$ Area/perimeter^{2}," and represented the mitochondria length and branching degree. An FF value of 1 indicated round and non-branched mitochondria, whereas a value less than 1 indicated longer and more branched mitochondria. The AR value was calculated as the ratio of the length of the long axis to that of the short axis, and represented the length of mitochondria. An AR value of 1, indicated a round mitochondrion. The value of AR increased with the length and elliptical shape of mitochondria. Based on the above, the FF and AR values tend to be close to 1 in damaged mitochondria [18].

3.3. Mitochondrial membrane potential assay

According to the instructions of the mitochondrial membrane potential assay kit using JC-1 (C2006; Beyotime), the culture medium was removed, and cells were washed with PBS (Beyotime) twice. The cell medium and JC-1 staining solution were mixed at a 1:1 ratio and then added to cells and incubated at 37 °C for 20 min. After incubation, the supernatant was removed. The appropriate cell medium was added, and cells were observed under a fluorescence microscope (DMi8; Leica). When the mitochondrial membrane potential is high, JC-1 forms J-aggregates; however, when the mitochondrial membrane potential is low, JC-1 remains in its monomeric form.

3.4. Mitochondrial stress

Seahorse XF cell culture microplates were seeded with the appropriate cell growth medium at a predetermined and optimized density. A sensor probe plate was hydrated with Seahorse XF calibration solution overnight in a CO_2-free incubator at 37 °C. All assay solutions and working fluids were prepared in advance according to the instructions of the mitochondrial stress test kit (Cat.103015-100; Agilent, CA, USA). Treated cells were washed with the assay solution twice, and then soaked in 500 μL of the assay solution, followed by incubation in a CO_2-free incubator at 37 °C for 1 h. Working fluids containing oligomycin, FFCP, and rotenone/antimycin were preadded to the sensor probe plate. Finally, the mitochondrial stress of the treated cells was detected using the Seahorse XFe24 Analyzer (Agilent).

3.5. ATP assay

According to the instructions of the ATP colorimetric/fluorometric assay kit (Cat.MAK190; Sigma), cells or myocardial tissue were quickly homogenized and filtered using a spin filter (Cat.UFC5010BK; Millipore, MA, USA), and then centrifuged at 14,000 *g* for 5 min. The supernatant was aspirated for subsequent tests. ATP standards, samples, and the reaction mix were separately added to black plates, mixed, and incubated at 25 °C away from light for 30 min. The absorbance was measured using a microplate reader (SpectraMax®i3x; Molecular Devices, CA, USA).

3.6. Determination of superoxide levels

To detect the level of superoxide in the mitochondria, cells were incubated with 5 μM MitoSox red mitochondrial superoxide indicator (Cat.40778ES50; YEASON) at 37 °C away from light for 30 min. Following washing, cells were incubated with the labeling solution of 200 nM Mito-Tracker green (Cat.C1048; Beyotime) at 37 °C away from light for 20 min. After rinsing, cells were observed under a laser scanning confocal microscope (SP5; Leica).

For the detection of intracellular superoxide, 5 μM dihydroethidium (Cat.S0063; Beyotime) was added to each well, and then cells were incubated at 37 °C away from light for 30 min. After washing, cells were observed under a conventional fluorescence microscope (Olympus, Tokyo, Japan).

To determine the presence of superoxide in myocardial tissues, heart tissue was removed from liquid nitrogen and slightly thawed at 25 °C and then cut into 10-μm-thick slices. According to the instructions of the ROS assay kit (Cat.S0033S; Beyotime), heart tissue sections were fully covered with 10 μmol/L of the fluorescent probe dye and incubated at 37 °C away from light for 20 min. After washing, sections were panoramically scanned under the Tissue FAXS Platform (Tissue Gnostics; Vienna, Austria). Myocardial nuclei displayed blue fluorescence, whereas superoxide was indicated by green fluorescence.

For further quantification, the content of myocardial ROS was detected. The heart tissues were weighed, washed with PBS, and then fully homogenized on ice. According to the manufacturer's instructions of the tissue ROS assay kit (Cat.HR8835; Biorab, Beijing, China), the homogenate was centrifugated at 1000×*g* and 4 °C for 10 min. A mixture containing 200 μl homogenate supernatant mixed with 2 μl probe was added to each well and incubated at 37 °C away from light for 30 min. The fluorescence intensity (FI) was measured using a fluorescence microplate reader (SuPerMax 3000FA; FLASH, Shanghai, China).

3.7. Measurement of calcium ions

For the mitochondrial calcium ions assay, 8-μM Rhod-2 AM, a fluorescent Ca^{2+} indicator (Cat.ab142780; Abcam, Cambridge, England) was added to each well at the end of cell treatment. Following removal of the dye, cells were washed, incubated with the labeling solution of 200 nM Mito-Tracker green (Cat.C1048; Beyotime) at 37 °C away from light for 20 min, and observed under a laser scanning confocal microscope (SP5; Leica).

For the measurement of intracellular calcium ions, cells were washed and incubated with a labeling solution containing 5 μM Fluo-3 AM, a fluorescent Ca^{2+} indicator (Cat.S1056; Beyotime) at 37 °C away from light for 30 min. After washing, cells were observed with a conventional fluorescence microscope (Olympus).

3.8. Mitochondrial transition pore assay

Cells were washed and then covered with labeling solution

containing 1.0 μM Hoechst 33342 dye, 1.0 μM calcein AM, 0.2 μM MitoTracker Red CMXRos, and 1.0 mM CoCl2 according to the protocol of the mitochondrial transition pore assay kit (Cat.I35103; Thermo Fisher Scientific). Cells were incubated at 37 °C away from light for 15 min. After washing, cells were observed under a conventional fluorescence microscope (Olympus). Calcein AM staining showed green fluorescence; stronger fluorescence indicated less opening of the mitochondrial permeability transition pore.

3.9. Fluorescence detection of apoptosis

According to the protocol of the annexin-V-FITC cell apoptosis detection kit (Cat.C1062L; Beyotime), Hoechst staining solution (Cat.33342; Beyotime), Annexin-V-FITC staining solution, and Propidium Iodide (PI) were added to the culture medium at the end of cell treatment, and cells were incubated at 37 °C away from light for 15 min. Following staining, the dye solution was discarded, cells were washed, and following the addition of fresh medium, they were observed under a conventional fluorescence microscope (Dmi8; Leica). Apoptotic cells exhibited dense or fragmented staining of the nuclei under Hoechst staining and showed green fluorescence upon annexin-V-FITC staining. Cells with ruptured membranes showed red fluorescence upon propidium iodide staining.

3.10. Echocardiographic assessment

Mice were anesthetized with 2% isoflurane (R510-22-8; RWD, Shenzhen China) and placed in a supine position. Cardiac function was evaluated using an imaging system (EPIQ7; Philips, Amsterdam, Netherlands). Upon M-mode and 2D tracing, the following parameters were measured: interventricular septal thickness at diastole (IVSd), left ventricular internal dimension at diastole (LVIDd), left ventricular posterior wall thickness in diastole (LVPWd), interventricular septal thickness in systole (IVSs); left ventricular internal dimension in systole (LVIDs), left ventricular posterior wall thickness in systole (LVPWs), end-diastolic volume index (EDV), end-systolic volume index (ESV), stroke volume (SV), fractional shortening (FS), ejection fraction (EF) and left ventricular mass (LV Mass).

3.11. Enzyme-linked immunosorbent assay (ELISA)

The detection of cardiac troponin I (cTnI) was performed using a mouse cTnI ELISA kit (Cat.ml001932; mlbio, Shanghai, China) according to the instructions of the manufacturer. A volume of 50 μL of serum, sample, or standard was added to each well. Subsequently, 100 μL of enzyme conjugate was added to the sample and standard wells, but not the blank well, and the plate was incubated for 60 min at 37 °C away from light. After washing, 50 μL of substrates A and B were added to each well and incubated for 15 min at 37 °C away from light. Finally, reactions in each well were terminated with 50 μL of termination solution. The OD value was measured using an enzyme reader (RT-6100; Rayto, Shenzhen, China).

3.12. Immunoblotting analysis

Cardiac tissues were lysed with RIPA lysis reagent (Cat. P0013B; Beyotime) containing protease (Cat. AR1179; Boster, CA, USA) and phosphatase (Cat.AR1183; Boster) inhibitors, homogenized on ice, and centrifuged at 14,000 g and 4 °C for 15 min. The protein concentration was determined using the bicinchoninic acid (BCA) method (Cat. AR0146; Beyotime). Proteins were separated in a suitable concentration of sodium dodecyl sulfate-polyacrylamide (Cat.C631100-0200; BBI; BBI, Shanghai, China) according to their molecular weight, and then transferred onto a polyvinylidene difluoride (PVDF, Cat. IPVH00010; Millipore) membrane using the Trans-Blot TurboTM System (Cat. 1704150; Bio-Rad, CA, USA). Nonspecific binding sites on the membrane were blocked using the QuickBlock™ blocking buffer for western blotting (Cat.P0252; Beyotime). Membranes were incubated at 4 °C overnight with the following primary antibodies: cytochrome C (cyt-c, Cat. AF0146, 1:1000; Affinity, Jiangsu, China), cleaved caspase-9 (Cat.9507, 1:1000; Cell Signaling, MA, USA), cleaved caspase-3 (Cat.9661, 1:2000; Cell Signaling), cleaved caspase-7 (Cat.9491; 1:1000; Cell Signaling), apoptosis-inducing factor (AIF, Cat.sc-13116; 1:1000; Santa Cruz, CA, USA), fatty acid transport protein 1 (FATP1, Cat.DF7716, 1:2000; Affinity), cluster of differentiation 36 (CD36, Cat.DF13262, 1:2000; Affinity), fatty acyl coenzyme A synthetase (FACS, Cat.4047s, 1:1000; Cell Signaling), carnitine palmityl transferase 1 (CPT-1, Cat.15184-1-AP, 1:1000; Proteintech, IL, USA), medium chain acyl-CoA dehydrogenase (MCAD, Cat.55210-1-AP, 1:1000; Proteintech), glucose transporter 4 (GLUT4, Cat.ab654, 1:1000; Abcam), complex I (COX I, cat.19703-1-AP, 1:1000; Proteintech) and complex IV (COX IV, cat.ab14744, 1:1000; Abcam). The expression of all detected proteins was normalized to that of β-actin (Cat.A2103, 1:1000; Sigma). Subsequently, membranes were soaked in anti-mouse (Cat.BA1050, 1:5000; Boster) or anti-rabbit (Cat. BA1055, 1:5000; Boster) secondary antibodies at 25 °C for 1 h. The ChemiDoc imaging system (Bio-Rad) was used for blot imaging.

3.13. COX I and COX IV enzyme activity assay

Complex I Enzyme Activity Assay Kit (Cat.ab109721, Abcam) and Complex IV Enzyme Activity Assay kit (Cat.ab109911, Abcam) were performed according to the manufacturer's instructions. Briefly, the heart tissue was homogenized in ice cold PBS or solution 1, and the homogenized tissue was adjusted to 5.5 mg/ml with PBS or solution 1. A 1/10 volume of detergent solution was added in the sample for extracting the proteins. After centrifugation at 16,000 rpm for 20 min at 4 °C, the supernatant was collected and diluted to 100 μg/ml or 500 μg/ml. Samples were loaded on plates and incubated for 3 h at room temperature. The assay wells were rinsed twice and the appropriate volume of assay solution was added in them. For the Complex I Enzyme Activity Assay, OD_{458} measurements were obtained at 1 min intervals for 30 min at room temperature. Subsequently, OD_{550} measurements were obtained at 1 min intervals for 2 h at 30 °C for the Complex IV Enzyme Activity Assay.

3.14. TMRE mitochondrial membrane potential assay

Mitochondria from heart tissue were isolated using the Minute™ Muscle tissue and Cell Mitochondrial Extraction Kit (Cat. MM-038, Invent). According to the manufacturer's instructions, cardiac tissue was initially homogenized in buffer A; some homogenate was reserved for BCA protein quantification and the rest was centrifuged at 16,000 rpm for 30s. The precipitate was rotated in order to re-suspend, and was centrifuged again at 1000 rpm for 5 min. Following centrifugation, the supernatant was collected and centrifuged at 11,000 rpm for 20 min. Buffer B was added to the precipitation, and following resuspension the solution was centrifuged at 11,000 rpm for 10 min. The supernatant was then transferred to a new centrifuge tube, and 0.3 ml of pre-cooled PBS were added to the tube. Following thorough mixing, the solution was centrifuged at 16,000 rpm for 20 min; the precipitate of this centrifugation was the isolated mitochondria. 500 nM tetramethylrhodamine ethyl ester (TMRE) working solution was added into the mitochondria-containing pellet, the pellet was thoroughly resuspended, and incubated at room temperature for 30 min. After washing, the mitochondria were resuspended and added into plate, and were functionally assessed using a microplate reader (SpectraMax®i3x; Molecular Devices, CA, USA).

3.15. Quantification and statistical analysis

Data are presented as mean ± standard error of the mean. Statistics were analyzed using the SPSS software (version 25.0; SPSS, Chicago, IL, USA), whereas data was visualized with the GraphPad Prism 7.0

software (GraphPad, San Diego, CA, USA). The two-way non-repeated-measures analysis of variance (ANOVA) was used for testing the effects of PA, ISO, and their interactions. The one-way ANOVA was used for comparing other experimental groups when data conformed to a normal distribution or used the Kruskal-Wallis rank sum test for abnormal distribution. Statistical significance was set at $P < 0.05$.

4. Results

4.1. High fatty acid environment attenuated the resistance of cardiomyocytes to isoproterenol

To simulate the state of fatty acid metabolism in the diabetic myocardium, we exposed cardiomyocytes to high concentrations of PA [11]. As indicated by the CCK-8 assay, the viability of cardiomyocytes was gradually increased following exposure to high concentrations of PA for 8 h ($P < 0.05$ and $P < 0.01$, respectively; Fig. 1A) but then decreased upon the 12th hour of exposure ($P < 0.05$; Fig. 1A). Therefore, following exposure to PA for 4 h, cardiomyocytes were treated with the ISO β-adrenoceptor agonist. Compared with the BSA control group, the viability of BSA-pretreated cardiomyocytes was increased after treatment with 1 mmol/L (mM) and 2 mM ISO for 2 h ($P < 0.001$ and $P < 0.001$, respectively; Fig. 1B) but decreased when the concentration of ISO reached 4 mM ($P < 0.01$; Fig. 1B). Regarding PA-pretreated cells, although treatment with 1 mM ISO for 2 h still promoted cell viability, treatment with 2 mM ISO did not affect this parameter ($P < 0.05$; Fig. 1B). In contrast, compared with 2 mM ISO in the BSA group, 2 mM ISO decreased cell viability in the PA group ($P < 0.05$; Fig. 1B). The same result was obtained in the PA group when treated with 4 mM ISO compared with to treatment with 4 mM ISO in the BSA group ($P < 0.01$; Fig. 1B). Although treatment with 2 mM ISO for 4 h had no significant effect on the viability of BSA-pretreated cells, it significantly inhibited the viability of PA-pretreated cells compared with the PA control group and 2 mM ISO in the BSA group ($P < 0.001$ and $P < 0.01$, respectively; Fig. 1C). Moreover, when treatment was prolonged to 12 h, cell viability was decreased in all groups ($P < 0.001$; Fig. 1D). Then, the 1 mM ISO-induced inhibition on the viability of PA-pretreated cardiomyocytes was greater than that in BSA-pretreated cells ($P < 0.001$; Fig. 1D). The

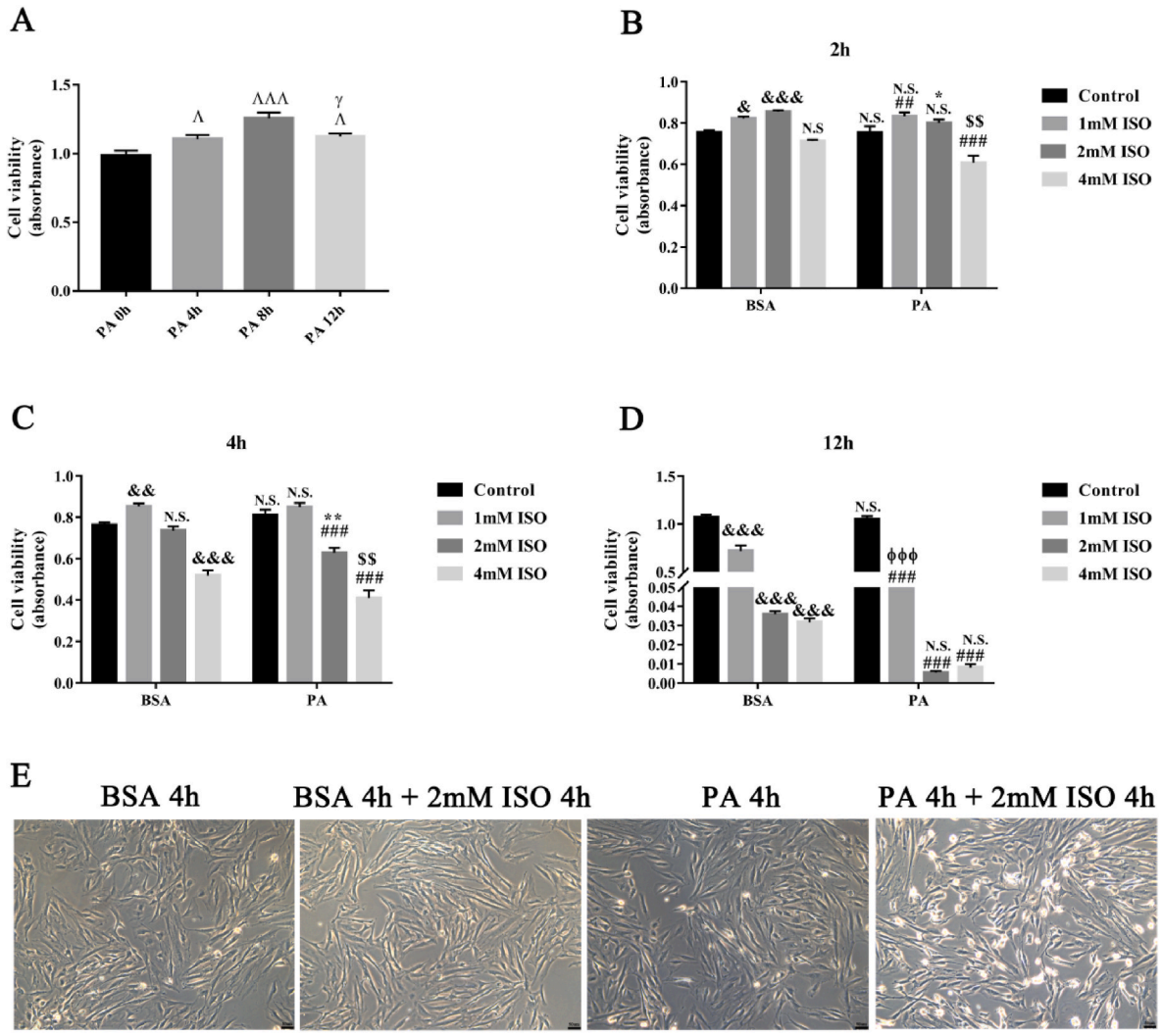

Fig. 1. A high-content fatty acid environment attenuates the resistance of cardiomyocytes to isoproterenol. (A) Upon administration of 500 μM PA on cardiomyocytes for different exposure times (0, 4, 8, 12 h), cell viability was evaluated using the CCK-8 kit. (B–D) Cardiomyocytes pretreated with 500 μM PA or 0.5% BSA for 4 h, were further treated with ISO (1, 2, 4 mM) for different times (2, 4, 12 h), and cell viability was determined using the CCK-8 kit. (E) Representative morphological images of cardiomyocytes under selected treatment conditions; Scale bar = 50 μm control in PA *vs* control in BSA; 1 mM ISO in PA *vs* BSA and 1 mM ISO in BSA; 2 mM ISO in PA *vs* BSA and 2 mM ISO in BSA; 4 mM ISO in PA *vs* BSA and 4 mM ISO in BSA; $^{\Lambda}P < 0.05$, $^{\Lambda\Lambda\Lambda}P<0.001$ *vs* PA 0 h; $^{\gamma}P<0.05$ *vs* PA 8 h; $^{\&\&}P < 0.01$, $^{\&\&\&}P < 0.001$ *vs* control in BSA; $^{\#}P < 0.05$, $^{\#\#\#}P < 0.001$ *vs* control in PA; $^{*}P < 0.05$, $^{**}P < 0.01$, $^{***}P < 0.001$ *vs* 2 mM ISO in BSA; $^{\$\$}P < 0.01$, $^{\$\$\$}P < 0.001$ *vs* 4 mM ISO in BSA; N.S. means not significant. BSA, bovine serum albumin; PA, Palmitic acid; ISO, isoproterenol.

treatment with 2 mM ISO for 4 h sufficiently imitated SH-induced myocardial injury in diabetic mice, but had no obvious effect on nondiabetic mice. Therefore, in the following experiment, BSA- or PA-pretreated cardiomyocytes were treated with or without 2 mM ISO for 4 h (Fig. 1E). Fatty acid-pretreated cardiomyocytes are more susceptible to damage, potentially due to the overactivation of β-adrenoceptors.

4.2. High fatty acid metabolism promoted mitochondrial structural and functional damage after β-adrenoceptor activation in cardiomyocytes

We examined the morphology and function of mitochondria in cardiomyocytes to observe the changes in energy metabolism. The AR and FF values tend to be close to 1 in round and non-branched damaged mitochondria [18]. Compared with the BSA group, the BSA + ISO group had greater AR and less FF values, indicating that ISO increased the length and number of branches of mitochondria ($P < 0.01$; Fig. 2A-2C). However, compared with the BSA + ISO and PA groups, the PA + ISO group was associated with less AR and greater FF values, indicating that the length and number of branches of mitochondria were decreased in the PA + ISO group. ($P < 0.001$ and $P < 0.01$, respectively; Fig. 2A–C). To further explore the mitochondrial function in cardiomyocytes, we measured the mitochondrial membrane potential and the oxidative respiration rate. The mitochondrial membrane potential assay (Fig. 2D) revealed that ISO did not affect the mitochondrial membrane potential of BSA-pretreated cardiomyocytes, whereas the mitochondrial membrane potential was significantly reduced in PA-pretreated cells compared with that in the BSA + ISO and PA groups ($P < 0.001$ and $P < 0.001$, respectively; Fig. 2E). The evaluation of oxygen consumption rate (OCR) of cardiomyocytes (Fig. 2F) showed that compared with the BSA group, basal respiration increased in the PA group ($P < 0.05$; Fig. 2G), but decreased in the PA + ISO group, compared with the BSA + ISO and PA groups ($P < 0.01$, $P < 0.001$, respectively; Fig. 2G). The maximal respiration also increased in the PA group compared with the BSA group ($P < 0.01$; Fig. 2H), but decreased in the PA + ISO group compared with the BSA + ISO and PA groups ($P < 0.01$; Fig. 2H). The spare respiratory capacity increased in the ISO and PA groups compared with the BSA group ($P < 0.05$; Fig. 2I), and decreased in the PA + ISO group compared with the BSA + ISO and PA groups ($P < 0.05$; Fig. 2I). Consistently, ATP production derived from oxidative phosphorylation increased in the PA group ($P < 0.05$; Fig. 2J) but decreased in the PA + ISO group, compared with the BSA + ISO and PA groups ($P < 0.01$, $P < 0.001$, respectively; Fig. 2J). Our evaluation of the total ATP content of cardiomyocytes suggested that compared with the BSA group, the production of total ATP was increased in both the BSA + ISO and PA groups ($P < 0.01$, $P < 0.001$; Fig. 2K). However, compared with the BSA + ISO and PA groups, ISO significantly reduced the total ATP content in PA-pretreated cells ($P < 0.01$, $P < 0.01$, respectively; Fig. 2K).

4.3. High fatty acid metabolism promoted oxidative stress and calcium overload from mitochondria to cytoplasm after β-adrenoceptor activation in cardiomyocytes

To explore the mechanism by which high fatty acid metabolism aggravates ISO-induced myocardial cell damage, we detected the levels of intracellular and mitochondrial superoxide and Ca^{2+}, both of which play pivotal roles in the physiological and pathological processes of lipid metabolism and β-receptor hyperactivation in the myocardium [11, 19–21]. Upon MitoSOX staining, which compared the PA with the BSA group, the PA group was characterized by an elevation in the levels of mtROS ($P < 0.001$; Fig. 3A and B). Specifically, ISO not only increased the production of ROS in the mitochondria of BSA-pretreated cardiomyocytes but further aggravated the burst of ROS in the mitochondria of PA-pretreated cells ($P < 0.05$, $P < 0.001$, respectively; Fig. 3A and B). Moreover, compared with the BSA + ISO group, the PA + ISO group also exhibited a higher production of mtROS ($P < 0.001$; Fig. 3A and B). However, compared with the BSA + ISO and PA groups, the PA + ISO group showed a higher level of intracellular ROS ($P < 0.001$; Fig. 3C and D), whereas, compared with the BSA group, no obvious changes were found in the BSA + ISO and PA groups (Fig. 3C and D). Rhode-2 AM staining similarly showed an increase in the level of mitochondrial Ca^{2+} only in the PA + ISO group compared with the BSA + ISO and PA groups ($P < 0.001$ and $P < 0.001$, respectively; Fig. 3E and F). PA promoted the production of cellular Ca^{2+} ($P < 0.01$; Fig. 3G and H), compared with the BSA group. However, although the intracellular level of Ca^{2+} was increased in both BSA- and PA-pretreated cardiomyocytes after treatment with ISO ($P < 0.001$ and $P < 0.05$, respectively; Fig. 3G and H), no significant difference was found between the BSA + ISO and PA + ISO groups (Fig. 3G and H).

4.4. High fatty acid metabolism promoted nonapoptotic damage after β-adrenoceptor activation in cardiomyocytes

Accumulation of ROS and $Ca^{2+}$is a key factor for inducing apoptosis through the stimulation of the opening of the mitochondrial membrane transition pore (mPTP) [22,23]. Thus, we examined the opening of the mPTP and related indicators of apoptosis. Contrary to our expectations, PA facilitated the opening of mPTP compared with the BSA group, showing lower fluorescence intensity of calcein AM ($P < 0.01$, Fig. 4A and B). In contrast, ISO induced the closure of mPTP in both BSA- and PA-pretreated cardiomyocytes, and was associated with higher fluorescence intensity of calcein AM ($P < 0.001$; Fig. 4A and B); this effect was stronger in the BSA-pretreated cells compared with the PA-pretreated cells ($P < 0.001$; Fig. 4A and B). Fluorescent staining using Hoechst, Annexin-V, and PI revealed the lack of any obvious agglutination of chromatin, phosphatidylserine eversion, or loss of cell membrane integrity among the four groups (Fig. 4C). The levels of apoptosis-related proteins were further evaluated by western blotting (Fig. 4D). The expression of cyt-c in the PA + ISO group was lower than that in the PA group ($P < 0.05$, Fig. 4E), as indicated in our Western blot analyses. Although we did not detect any differences in the expression of cleaved caspase-9 between the PA + ISO and PA groups, the expression of cleaved caspase-9 in the PA + ISO group was relatively higher than that in the BSA + ISO group ($P < 0.05$, Fig. 4E), as ISO reduced the expression of cleaved caspase-9 in BSA-pretreated cardiomyocytes ($P < 0.01$, Fig. 4F). The expression of cleaved caspase-3 was not significantly different among the four groups (Fig. 4G). Compared with the BSA group, both the BSA + ISO and PA groups showed a decreased expression of cleaved caspase-7 ($P < 0.05$, $P < 0.001$; Fig. 4H). Meanwhile, we did not observe any changes in the expression of AIF, a caspase-independent apoptosis-related protein (Fig. 4I). Based on previous findings, we speculated that PA aggravates the ISO-induced cardiomyocyte damage, which might be related to ferroptosis. Therefore, we administered different concentrations of Fer-1 and DFO to observe the cooperative effect of PA and ISO on cardiomyocyte damage. Both 50 nM Fer-1 and 30 μM DFO effectively reversed the PA- and ISO-induced decrease in the activity of cardiomyocytes ($P < 0.05$, $P < 0.01$; Fig. 4J–L).

Mito-TEMPO protected cardiomyocytes from damage induced by the synergistic effect Considering that the level of mtROS was significantly altered upon different treatments, we speculated that high fatty acid metabolism might weaken the resistance of cardiomyocytes to ISO through mtROS. Upon administration of MT, an mtROS scavenger in high fatty acid environments, the resistance of PA-pretreated cardiomyocytes to ISO was enhanced in varying degrees; especially under treatment with 50 μM MT for 2 h ($P < 0.01$; Fig. 5A and B). Furthermore, MT reduced the level of superoxide in the mitochondria ($P < 0.001$; Fig. 5C and D) and cytoplasm ($P < 0.001$; Fig. 5E and F) of injured cells. However, although MT rescued the PA and ISO coinduced mitochondrial Ca^{2+} overload ($P < 0.001$; Fig. 5G and H), its protective effect on cellular Ca^{2+} was not obvious (Fig. 5I and J).

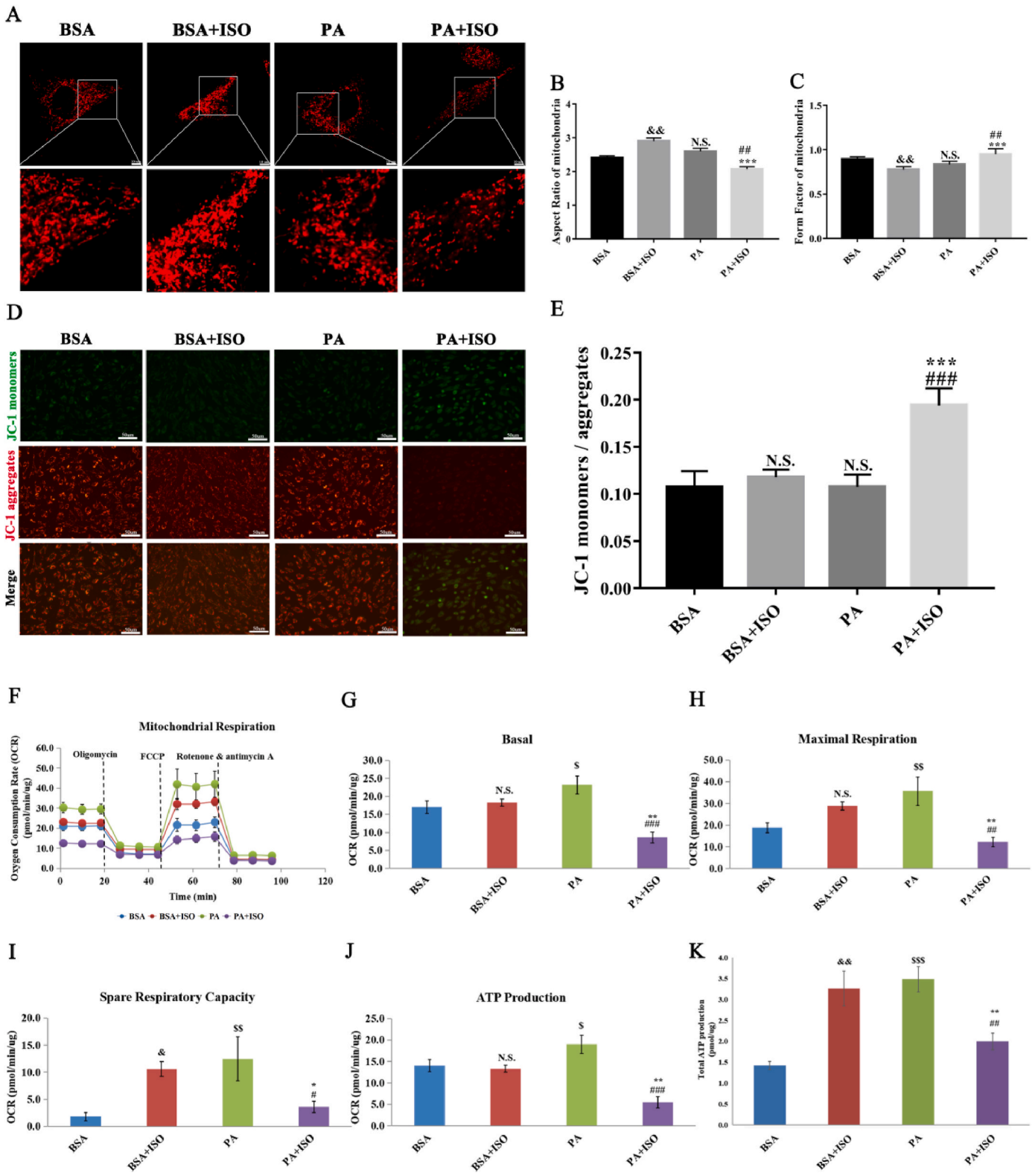

Fig. 2. High fatty acid metabolism promotes mitochondrial structural and functional damage after β-adrenoceptor activation in cardiomyocytes. (A) Mitochondrial staining with MitoTracker Red; Scale bar = 10 μm. (B, C) The calculation of mitochondrial morphological parameters of image 2A. The FF and AR values tend to be close to 1 in damaged mitochondria. (D) Mitochondrial membrane potential was assayed using the JC-1 kit; Scale bar = 50 μm. (E) Quantification of relative fluorescence intensity of JC-1. (F) Seahorse XFe24 Analyzer detected the oxygen consumption rate using the mitochondrial stress test kit. (G–J) Quantification of mitochondrial respiration based on image 2F, including basal respiration, maximal respiration, spare respiration capacity, and ATP production. (K) Detection of total ATP production using an ATP colorimetric/fluorometric assay kit. Cells were pretreated with 500 μM PA or 0.5% BSA for 4 h, and were subsequently treated with 2 mM ISO for another 4 h, before being subjected to the above readouts. BSA + ISO *vs* BSA; PA *vs* BSA; PA + ISO *vs* PA and BSA + ISO; $^{\&}P < 0.05$, $^{\&\&}P < 0.01$ *vs* BSA; $^{\$}P < 0.05$, $^{\$\$}P < 0.01$, $^{\$\$\$}P < 0.001$ *vs* BSA; $^{\#}P < 0.05$, $^{\#\#}P < 0.01$, $^{\#\#\#}P < 0.001$ *vs* PA; $^{*}P < 0.05$, $^{**}P < 0.01$, $^{***}P < 0.001$ *vs* BSA + ISO; N.S. means not significant. OCR, oxygen consumption rate; ATP, adenosine triphosphate.

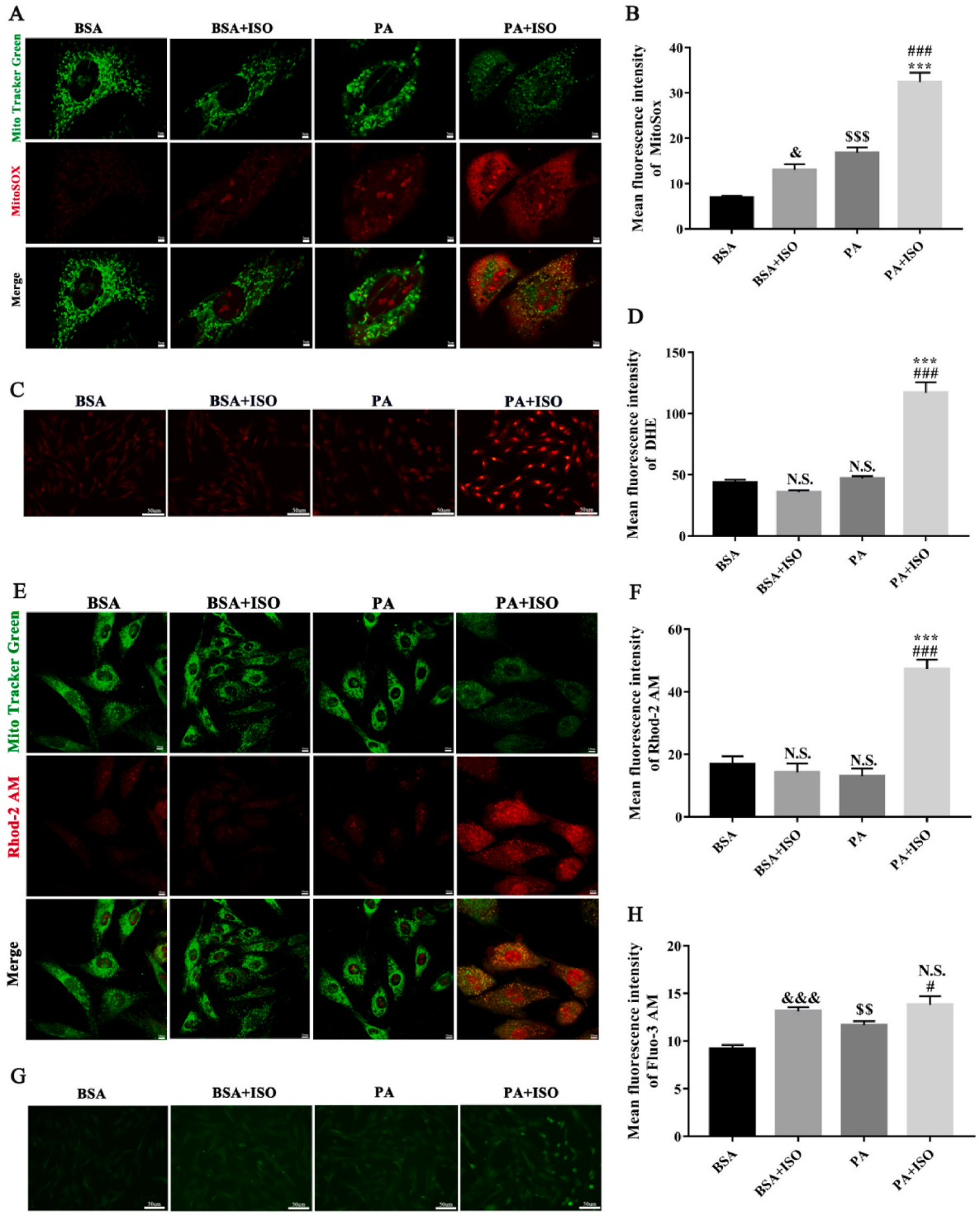

Fig. 3. High fatty acid metabolism promotes oxidative stress and calcium overload from mitochondria to cytoplasm after β-adrenoceptor activation in cardiomyocytes. (A) Mitochondrial localization using Mito-Tracker green and detection of mitochondrial ROS using MitoSOX; Scale bar = 5 μm. (B) Quantification of fluorescence intensity of MitoSOX based on image 3A. (C) Detection of intracellular ROS with DHE; Scale bar = 50 μm. (D) Quantification of fluorescence intensity of DHE based on image 3C. (E) Mitochondrial localization using Mito-Tracker green and detection of mitochondrial calcium using Rhod-2 AM; Scale bar = 10 μm. (F) Quantification of fluorescence intensity of Rhod-2 AM based on image E. (G) Detection of intracellular calcium with Fluo-3 AM; Scale bar = 50 μm. (H) Quantification of fluorescence intensity of Fluo-3 AM based on image G. Cells were pretreated with 500 μM PA or 0.5% BSA for 4 h, and were subsequently treated with 2 mM ISO for another 4 h, before being subjected to the above readouts. BSA + ISO *vs* BSA; PA *vs* BSA; PA + ISO *vs* PA and BSA + ISO; $^{\&}P < 0.05$, $^{\&\&\&}P < 0.001$ *vs* BSA; $^{\$\$}P < 0.01$, $^{\$\$\$}P < 0.001$ *vs* BSA; $^{\#}P < 0.05$, $^{\#\#\#}P < 0.001$ *vs* PA; $^{***}P < 0.001$ *vs* BSA + ISO; N.S. means not significant. DHE, dihydroethidium.

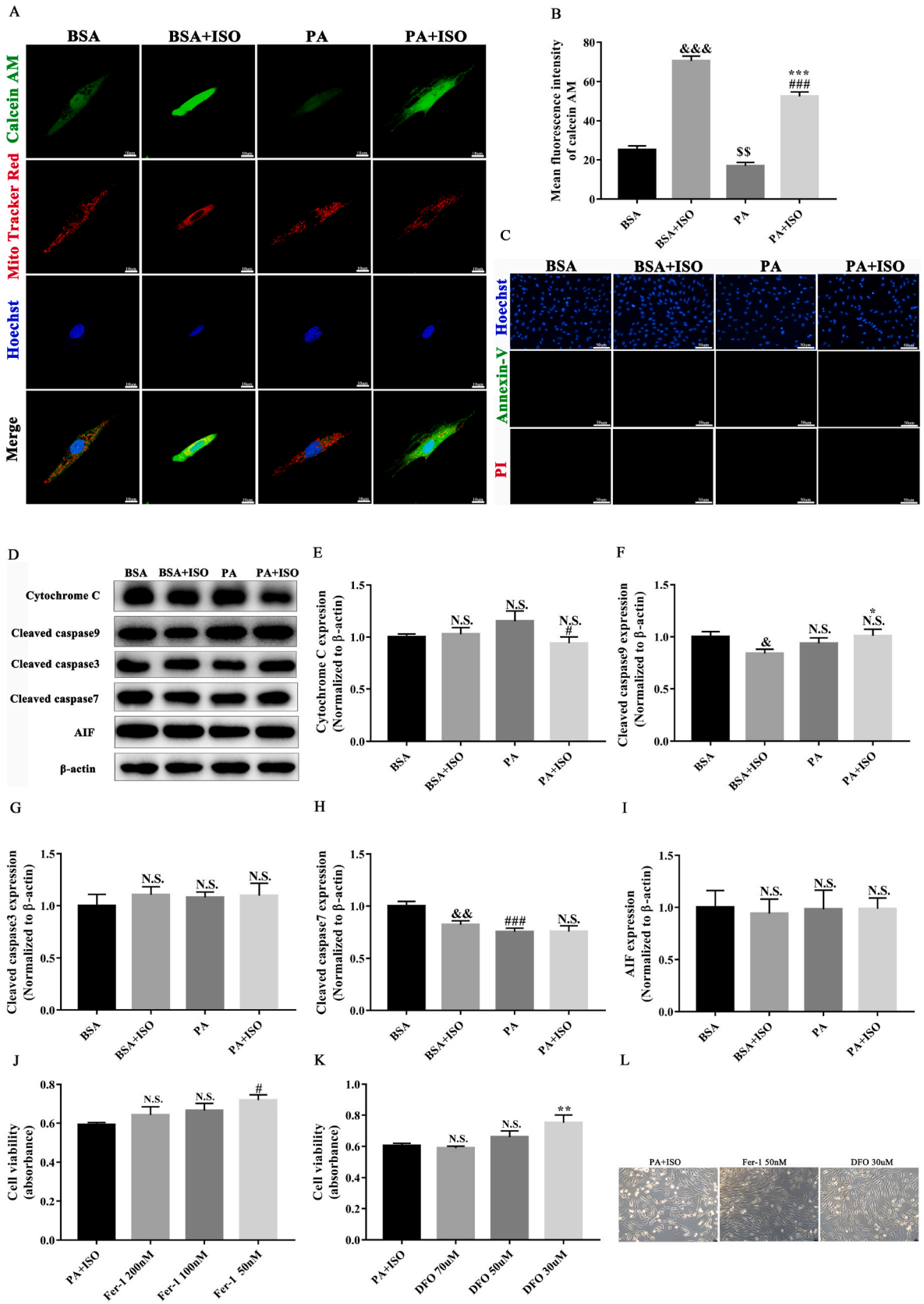

(caption on next page)

Fig. 4. High fatty acid metabolism promotes nonapoptotic damage after β-adrenoceptor activation in cardiomyocytes. (A) Evaluation of mPTP opening using calcien AM, mitochondrial localization using Mito-Tracker red, and nuclear localization using Hoechst; Scale bar = 10 μm. (B) Fluorescent quantification of calcien AM. (C) Nuclear staining using Hoechst, detection of phosphatidylserine exposure using annexin-V, and cell membrane integrity using PI; Scale bar = 50 μm. (D) Representative immunoblot image of proteins related to mitochondrial-dependent apoptosis. (E–I) Quantification of immunoblot image. (J–K) Effects of different concentrations of Fer-1 and DFO on the PA- and ISO-induced inhibition of cardiomyocyte viability. (L) Representative morphological image of cardiomyocytes attributable to model and treatment groups; Scale bar = 50 μm. Cells were pretreated with 500 μM PA or 0.5% BSA for 4 h, and were subsequently treated with 2 mM ISO for 4 h, before being subjected to the above readouts. Fer-1 (50, 100, 200 nM) and DFO (30, 50, 70 μM) were separately added at the same time when PA-pretreated (500 μM) cardiomyocytes received 2 mM ISO. BSA + ISO *vs* BSA; PA *vs* BSA; PA + ISO *vs* PA and BSA + ISO; $^{\&}P < 0.05$, $^{\&\&}P < 0.01$, $^{\&\&\&}P < 0.001$ *vs* BSA; $^{\$\$}P < 0.01$, $^{\$\$\$}P < 0.00$ *vs* BSA; $^{\#}P < 0.05$, $^{\#\#\#}P < 0.001$ *vs* PA; $^{*}P < 0.05$, $^{**}P < 0.01$, $^{***}P < 0.001$ *vs* BSA + ISO; (50, 100, 200 nM)Fer-1 *vs* PA + ISO; (30, 50, 70 μM)DFO *vs* PA + ISO; $^{\#}P < 0.05$ *vs* PA + ISO; $^{**}P < 0.01$ *vs* PA + ISO; N.S. means not significant. PI, propidium iodide; AIF, apoptosis-inducing factor; Fer-1, ferrostatin-1; DFO, deferoxamine mesylate.

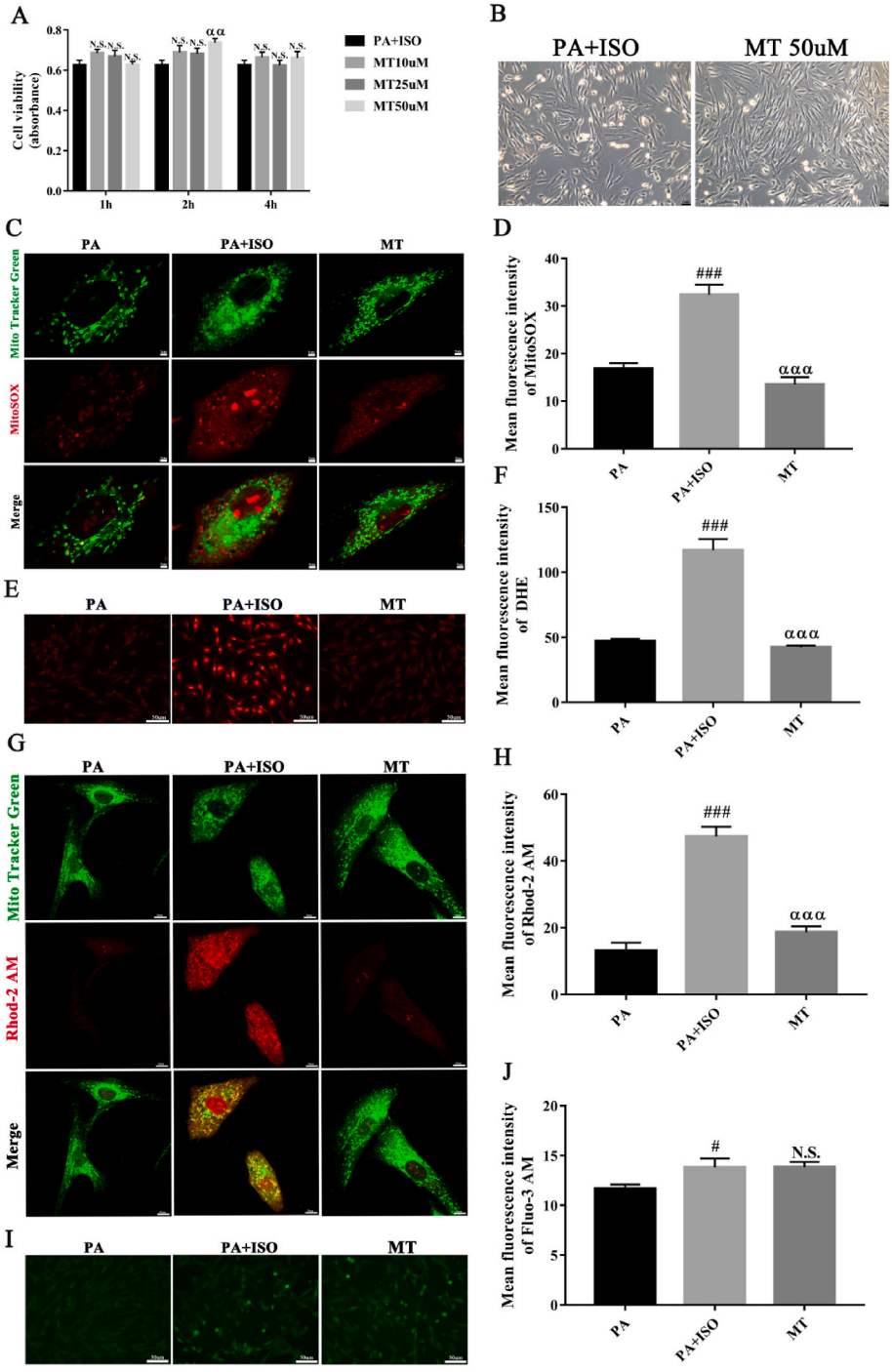

Fig. 5. Mito-TEMPO protects cardiomyocytes from damage induced by the synergistic effect. (A) Cells received administration of MT (10, 25, 50 μM) for various times (1, 2, 4 h) during PA pretreatment. After treatment with 2 mM ISO for 4 h, cell viability was evaluated using the CCK-8 kit (B) Representative morphological image of cardiomyocytes attributable to model and treatment groups; Scale bar = 50 μm. (C) Mitochondrial localization using Mito-Tracker green and detection of mitochondrial ROS using MitoSOX; Scale bar = 5 μm. (D) Detection of intracellular ROS; Scale bar = 50 μm. (E–F) Quantification of fluorescence intensity of mitochondrial and intracellular ROS based on images C and D. (G) Mitochondrial localization using Mito-Tracker green and detection of mitochondrial calcium using Rhod-2 AM; Scale bar = 10 μm. (H) Detection of intracellular calcium; Scale bar = 50 μm. (I–J) Quantification of fluorescence intensity of mitochondrial and intracellular calcium based on images G and H. Cells were pretreated or not with 50 μM MT for 2 h during the pretreatment with 500 μM PA; cells were then treated with 2 mM ISO for another 4 h, before being subjected to the above stainings. $^{\#}P < 0.05$, $^{\#\#\#}P < 0.001$ *vs* PA; $^{\alpha\alpha}P<0.01$, $^{\alpha\alpha\alpha}P<0.001$ *vs* PA + ISO. MT, Mito-TEMPO. DHE, dihydroethidium.

4.5. Mito-TEMPO protected the morphology and function of mitochondria of cardiomyocytes from damage induced by the synergistic effect

The PA and ISO coinduced reduction in the length and number of branches of the mitochondria was restored upon administration of MT ($P < 0.01$, $P < 0.05$, respectively; Fig. 6A-6C). Likewise, the PA and ISO coinduced inhibition of the mitochondrial membrane potential was also reversed by MT ($P < 0.01$; Fig. 6D and E). In agreement with the OCR of cardiomyocytes results (Fig. 6F), MT partially recovered the reduction in basal respiration ($P < 0.05$, Fig. 6G), maximal respiration ($P < 0.05$; Fig. 6H), and spare respiratory capacity ($P < 0.05$; Fig. 6I) induced by PA and ISO. The PA and ISO coinduced inhibition of ATP production showed a rebounding tendency ($P = 0.091$, Fig. 6J), and the decreased total production of ATP was managed by MT ($P < 0.05$; Fig. 6K).

4.6. Mito-TEMPO reduced myocardial ROS and improved cardiac dysfunction in diabetic mice after severe hypoglycemia

mtROS played a pivotal role in cardiac damage synergistically induced by high fatty acid metabolism and β-adrenoceptor activation. To identify the effect of mtROS scavengers in myocardial injury in diabetic mice after SH, we treated diabetic mice with MT and then subjected them to SH. There was no significant difference in the body weight and blood glucose levels among the three groups of mice before the induction of diabetes (Fig. 7A and B). On day 3 after STZ injection (i.e., the establishment of the diabetic model) all three groups exhibited decreased body weights and increased blood glucose levels compared with those before the induction of diabetes; however, no significant differences were noticed among the three groups ($P < 0.001$; Fig. 7A and B) until the day of sacrifice. Following i.p. injection of insulin, the blood glucose levels were significantly decreased in the DH and DHT groups, indicating SH lasting for 90 min (Fig. 7C). Fluorescent staining and quantitative detection of ROS revealed that following SH, the increase in ROS in diabetic mice pretreated with MT was inhibited ($P < 0.001$; Fig. 7D and E). Echocardiography showed that SH reduced the FS (%) and EF (%) in diabetic mice ($P < 0.01$, $P < 0.001$, respectively; Fig. 7F), whereas this effect was rescued by MT ($P < 0.001$; Fig. 7F). An increased LV mass in was observed in the DHT group compared with that in the DH group ($P < 0.01$; Fig. 7F). Consistent with this, SH promoted the elevation of cTnI in diabetic mice, which was reversed by MT ($P < 0.01$, $P < 0.001$, respectively; Fig. 7G).

4.7. Mito-TEMPO improved the severe hypoglycemia-impaired myocardial energy metabolism in diabetic mice

To further explore the effect of MT on myocardial metabolism in diabetic mice after SH, we examined the key proteins involved in fatty acid metabolism and glucose uptake in the myocardium using western blotting (Fig. 8A). SH inhibited the expression of CD36 and FATP1, the key protein of fatty acid uptake in the myocardium of diabetic mice ($P < 0.001$; Fig. 8B and C), whereas this effect was rescued by MT ($P < 0.01$; Fig. 8B and C). The protein expression of fatty acid oxidation markers, including CPT-1, FACS, and MCAD, was decreased in diabetic mice after SH ($P < 0.001$, $P < 0.01$, $P < 0.01$, respectively; Fig. 8D–F), whereas this effect was also reversed by MT ($P < 0.001$, $P < 0.05$, $P < 0.05$, respectively; Fig. 8D–F). MT effectively reversed the decrease in the level of GLUT4 induced by SH in diabetic mice ($P < 0.05$, $P < 0.01$, respectively; Fig. 8G). Then, we further investigated the mitochondrial function in the three groups. The detection of oxidative phosphorylation proteins (Fig. 8H) showed that SH didn't influence the expression of COX I (Fig. 8I) but decreased COX IV ($P < 0.01$; Fig. 8J), and this effect was rescued by MT ($P < 0.05$; Fig. 8J). However, we did not observe any changes on the activity of COX I and COX IV among the three groups (Fig. 8K and L). The evaluation of the mitochondrial potential and ATP content in myocardial tissues suggested that SH significantly reduced the mitochondrial potential and ATP production in diabetic mice ($P < 0.05$, $P < 0.01$, respectively; Fig. 8M and N), whereas this influence was prevented by MT ($P < 0.01$, $P < 0.001$ respectively; Fig. 8M and N). Overall, MT ameliorated the SH-induced inhibition of myocardial energy metabolism in diabetic mice.

5. Discussion

This study demonstrated that short-term exposure to a high fatty acid environment or β-adrenoceptor activation could stimulate the enhanced viability and energy metabolism of cardiomyocytes. However, When the two conditions were superimposed, pathological changes occur, they manifested as high fatty acid metabolism impairing the ability of cardiomyocytes to resist β-adrenoceptor hyperactivation, resulting in the induction of nonapoptotic damage. mtROS was found to be a key component in this synergistic effect. Reducing the level of mtROS in diabetic mice effectively prevented SH-induced cardiac dysfunction and energy metabolism damage.

In physiological conditions, the heart is an organ highly-dependent on fatty acid metabolism with flexible metabolic patterns [24]. In diabetes, as the concentration of free fatty acids elevates, the heart tends to increase fatty acid metabolism and further reduces insulin-dependent glucose requirements [10]. These metabolic characteristics of the heart indicate that changes in glucose may not be the primary factor responsible for adverse cardiac outcomes. Many clinical studies also support this speculation. For instance, clinical studies have shown that hemodynamic fluctuations, abnormal cardiac electrophysiology, hypercoagulability, and inflammatory responses closely related to catecholamines, are considered to be the potential culprits leading to adverse cardiovascular outcomes in diabetic patients, rather than changes in blood glucose [25]. Therefore, in our *in vitro* model, we administered β-receptor agonists instead of glycemic deprivation to investigate whether β-receptor activation of cardiomyocytes would result in differences in cardiomyocyte activity with and without high fatty acid metabolism. To explain the differential effect of hypoglycemia on myocardial outcomes, an in vivo model of diabetic and non-diabetic mice was also used. The rational for selecting our *in vitro* cell model was further validated by the uniformity of phenotypic changes observed between our *in vitro* and in vivo models. In this study, we activated β-receptor in cardiomyocytes preconditioned with or without high fatty acid metabolism, to model *in vitro* the myocardial high fatty acid metabolism observed in the diabetic state and the damage sympathetic hyperactivation induces to the cardiovascular system in hypoglycemia. We observed that increased fatty acid metabolism impaired the resistance of cardiomyocytes to β-receptor hyperactivation, resulting in decreased cellular activity and energy metabolism, accompanied by an increase in ROS. These changes are consistent with the cardiac outcome of the in vivo model of severe hypoglycemia in diabetic mice. When the lipid uptake of the myocardium is greater than its oxidation rate, excess lipid will accumulate in the heart damaging the myocardial tissue, thereby resulting in cardiac dysfunction, also known as myocardial lipid toxicity. In this study, cardiomyocytes with high fatty acid metabolism showed sensitivity to β-receptor activation even when their activity was not decreased. These observations suggest that in addition to lipotoxicity, a hypermetabolic pattern of cardiomyocytes may have been an independent risk factor.

Although previous studies have suggested that high fatty acid oxidation might be detrimental to cardiac function [13,26], the effect of this metabolic pattern on cardiac β-adrenoceptor activation remains to be elucidated. We discovered that high fatty acid metabolism weakened the cardiac resistance to β-adrenoceptor activation. This finding might largely explain the reason behind the aggravation of myocardial injury by SH in diabetic mice and the lack of this effect in nondiabetic mice. Moreover, patients with diabetes, metabolic syndrome, or obesity with high serum lipids might be more vulnerable to cardiovascular events following sympathetic activation originating from psychological,

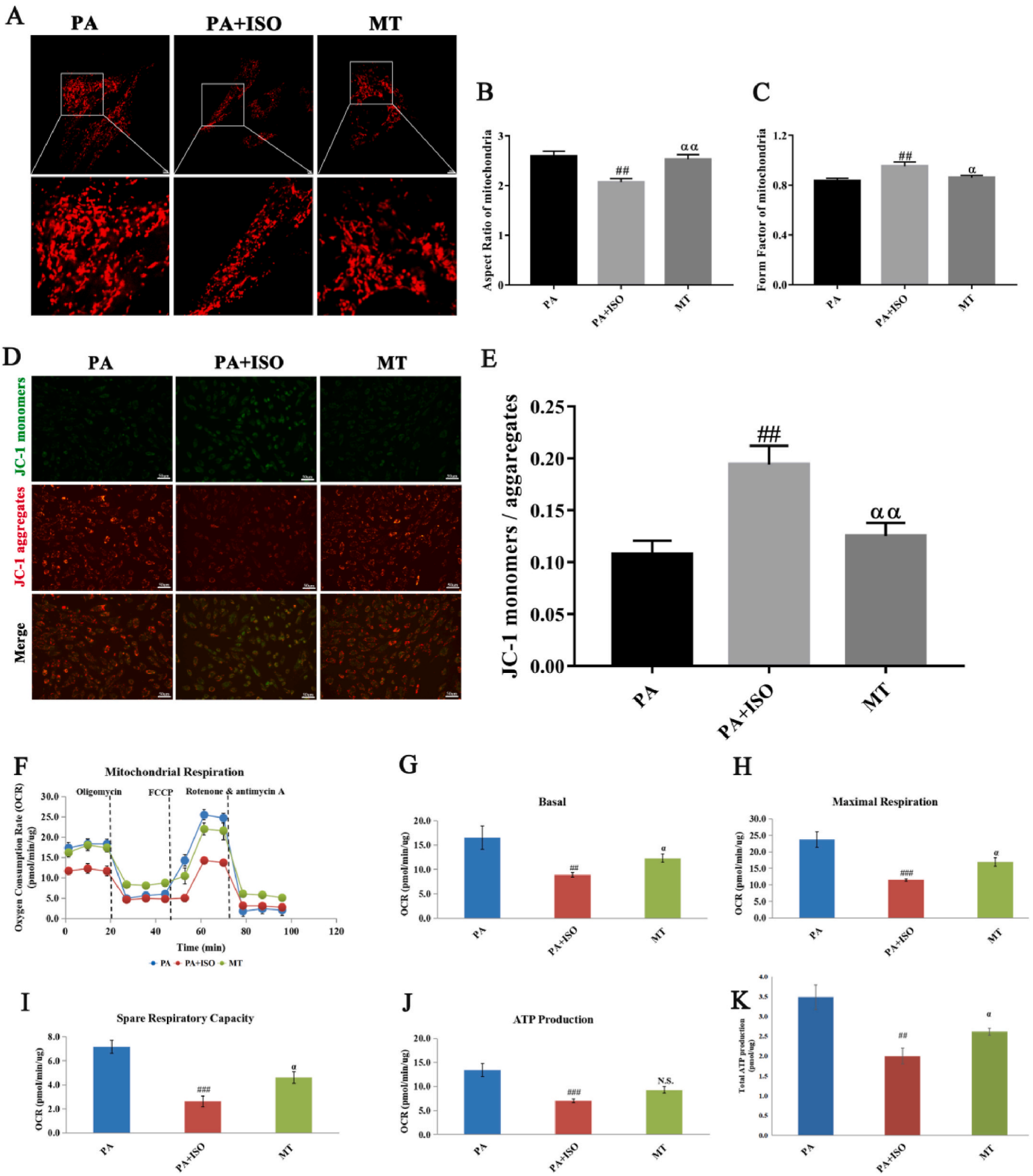

Fig. 6. Mito-TEMPO protects the morphology and function of mitochondria of cardiomyocytes from damage induced by the synergistic effect. (A) Mitochondrial staining with MitoTracker Red; Scale bar = 10 μm. (B, C) The calculation of mitochondrial morphological parameters of image 6A. The FF and AR values tend to be close to 1 in damaged mitochondria (D) Mitochondrial membrane potential was assayed with JC-1 kit; Scale bar = 50 μm. (E) Quantification of relative fluorescence intensity of JC-1. (F) Seahorse XFe24 Analyzer detected the oxygen consumption rate with mitochondrial stress test kit. (G–J) Quantification of mitochondrial respiration based on image 6F, including basal respiration, maximal respiration, spare respiration capacity and ATP production. (K) Detection of total ATP production with ATP colorimetric/fluorometric assay kit. Cells pretreated or not with 50 μM MT for 2 h during pretreatment of 500 μM PA, and treated with 2 mM ISO for 4 h, then received those staining. $^{\#}P < 0.05$, $^{\#\#}P < 0.01$, $^{\#\#\#}P < 0.001$ *vs* PA; $^{\alpha}P < 0.05$, $^{\alpha\alpha}P < 0.01$ *vs* PA + ISO. MT, Mito-TEMPO. OCR, oxygen consumption rate; ATP, adenosine triphosphate.

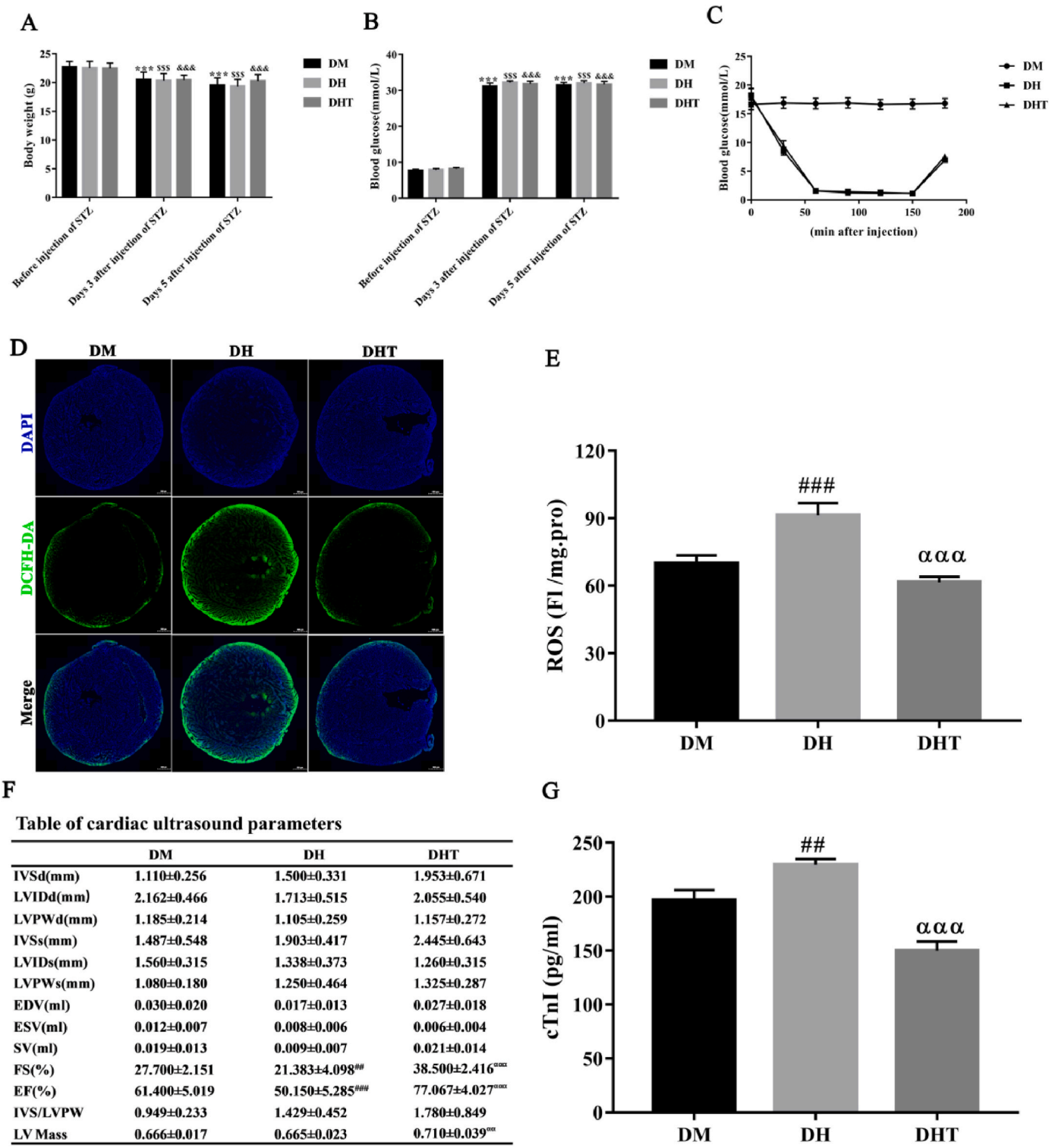

Table of cardiac ultrasound parameters

	DM	DH	DHT
IVSd(mm)	1.110±0.256	1.500±0.331	1.953±0.671
LVIDd(mm)	2.162±0.466	1.713±0.515	2.055±0.540
LVPWd(mm)	1.185±0.214	1.105±0.259	1.157±0.272
IVSs(mm)	1.487±0.548	1.903±0.417	2.445±0.643
LVIDs(mm)	1.560±0.315	1.338±0.373	1.260±0.315
LVPWs(mm)	1.080±0.180	1.250±0.464	1.325±0.287
EDV(ml)	0.030±0.020	0.017±0.013	0.027±0.018
ESV(ml)	0.012±0.007	0.008±0.006	0.006±0.004
SV(ml)	0.019±0.013	0.009±0.007	0.021±0.014
FS(%)	27.700±2.151	21.383±4.098$^{\#\#}$	38.500±2.416$^{\alpha\alpha\alpha}$
EF(%)	61.400±5.019	50.150±5.285$^{\#\#\#}$	77.067±4.027$^{\alpha\alpha\alpha}$
IVS/LVPW	0.949±0.233	1.429±0.452	1.780±0.849
LV Mass	0.666±0.017	0.665±0.023	0.710±0.039$^{\alpha\alpha}$

Fig. 7. Mito-TEMPO reduced myocardial ROS and improved contractile dysfunction in diabetic mice after severe hypoglycemia. (A–B) Body weight and levels of blood glucose among the three groups on day 1, day 3 and day 5 after injection of STZ (150 mg/kg). (C) Blood glucose monitoring during induction of 90 min severe hypoglycemia (<2.0 mmol/L). (D) Immunofluorescent images of cardiac tissues, including nuclear staining with DAPI and ROS staining with DCFH-DA. (E) Determination of ROS content in myocardial tissues using an ROS ELISA kit. (F) Cardiac ultrasound parameters of mice in the three groups. (G) Determination of the serum cTnI content using a mouse cTnI ELISA. Diabetic mice were treated with severe hypoglycemia for 90 min after pretreatment with MT (0.7 mg/kg/d), twice. The above evaluations were conducted at the 24th hour after the termination of hypoglycemia. $^{***}P < 0.001$ *vs* DM before injection of STZ; $^{\$\$\$}P < 0.001$ *vs* DH before injection of STZ; $^{\&\&\&}P < 0.001$ *vs* DHT before injection of STZ; $^{\#\#}P < 0.01$, $^{\#\#\#}P < 0.001$ *vs* DM; $^{\alpha\alpha\alpha}P<0.001$ *vs* DH. DM, mice with diabetes mellitus; DH, diabetic mice experiencing hypoglycemia; DHT, diabetic mice pretreated with Mito-TEMPO experiencing hypoglycemia; FI, fluorescence intensity; IVSd, interventricular septal thickness at diastole; LVIDd, left ventricular internal dimension at diastole; LVPWd, left ventricular posterior wall thickness in diastole; IVSs, interventricular septal thickness in systole; LVIDs, left ventricular internal dimension in systole; LVPWs, left ventricular posterior wall thickness in systole; EDV, end-diastolic volume index; ESV, end-systolic volume index; SV, stroke volume; FS, fractional shortening; EF, ejection fraction; LV Mass, left ventricular mass; cTnI, cardiac troponin I.

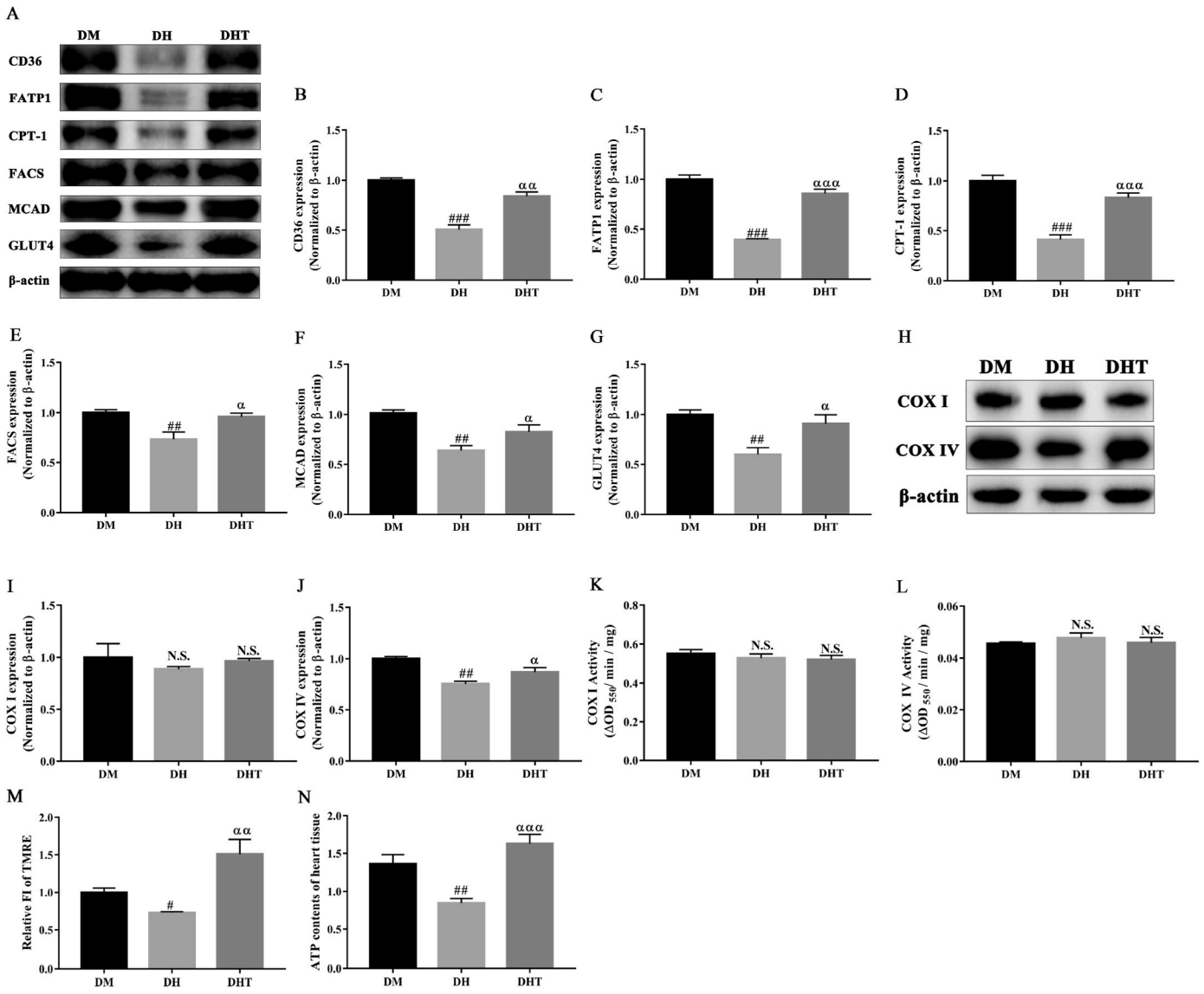

Fig. 8. Mito-TEMPO improves the myocardial energy metabolism impaired by severe hypoglycemia in diabetic mice. (A) Representative immunoblot image of proteins related to lipid metabolism and glucose uptake. (B–G) Quantification of immunoblot image. (H) Representative immunoblot image of proteins related to oxidative phosphorylation. (I–J) Quantification of immunoblot image. (K–L) Activity of the COX I and COX IV enzymes. (M) Determination of mitochondrial potential of myocardium. (N) Determination of ATP content in cardiac tissues. Diabetic mice were treated with severe hypoglycemia for 90 min after pretreatment with MT (0.7 mg/kg/d), twice. The above evaluations were performed at the 24th hour after the termination of hypoglycemia. $^{\#\#}P < 0.01$, $^{\#\#\#}P < 0.001$ *vs* DM; $^{\alpha}P<0.05$, $^{\alpha\alpha}P<0.01$, $^{\alpha\alpha\alpha}P<0.001$ *vs* DH.CD36, cluster of differentiation 36; FATP1, fatty acid transporter 1; CPT-1, carnitine palmityl transferase 1; FACS, fatty acyl coenzyme A synthetases; MCAD, medium-chain acyl-CoA dehydrogenase; GLUT4, glucose transporter 4; COX I, complex I; COX IV, complex IV; TMRE, tetramethylrhodamine ethyl ester.

physical, or environmental stress [12]. Abundant clinical studies support this hypothesis. For example, obesity-induced cardiac dysfunction and heart failure have also been closely related to sympathetic nerve activation [27]. Inhibition of lipolysis could effectively prevent ISO-induced heart failure [28]. However, it is worth considering that many confounding factors tend to co-present in patients. Therefore, it is difficult to clarify the mechanism underlying this synergistic effect between cardiac patterns of high fatty acid metabolism and sympathetic activation in inducing cardiovascular events in vivo. In our study, we first induced high fatty acid metabolism in cardiomyocytes, retaining their viability, and then stimulated β-adrenoceptor activation to observe whether these two physiological effects would produce pathological results, balancing the defect of the in vivo experiment.

Mitochondria play a crucial role in life processes, as they are involved in cellular energy production and the induction of apoptosis [29]. Normal mitochondrial structure and membrane potential provide the basis for maintaining their oxidative phosphorylation ability [30,31]. Mitochondria are the principal organelles that produce ROS, which is known to be increased with the enhancement of OXPHOS [14]. However, excessive ROS and its sensitization of mPTP to Ca^{2+} has been shown to induce mitochondrial dysfunction and cell apoptosis [32]. The β-adrenoceptor activation results in an increased influx of Ca^{2+}into myocytes, promoting a positive inotropic response, whereas β-adrenoceptor hyperactivation tends to result in cardiomyocyte damage characterized by Ca^{2+}overload and oxidative stress [33,34]. The opening of mPTP is principally triggered by Ca^{2+}, especially together with ROS, whereas it is inhibited by various factors, including a low pH, Mg^{2+}, adenine nucleotides, and CypD inhibitors, leading to mitochondrial damage and cell apoptosis [22,23]. Although we observed an abatement of mitochondrial membrane potential, oxidative phosphorylation, and

ATP synthesis accompanied by an overload of Ca^{2+} and ROS in our *in vitro* model, the mPTP did not open as expected but remained closed. Accordingly, the mitochondria did not show a massive outflow of apoptosis inducers. We speculated that this might be attributed to the exposure time and concentration of treatment agents or the consequence of negative regulatory factors. It can't be excluded that the closure of the mPTP might imply the manner of cell death, as the transient opening of the mPTP is beneficial to physiological regulation [35,36].

It is well known that structure and function are closely associated. Indeed the changes of cell morphology were greater than the observed functional changes, suggesting that the improvement of cell morphology following Mito-TEMPO pretreatment may precede the improvement in cell activity. The detection principle of cell activity is highly dependent on the activity and quantity of dehydrogenase within cells. Therefore, we speculate that the observed phenotype could be attributed to the activity or quantity of dehydrogenase within the cells not being increased in time. Whether Mito-TEMPO could further strengthen cell activity requires more exploration, such as additional pretreatments of Mito-TEMPO with higher concentrations at each time point, in order to observe changes in cell activity.

Ferroptosis is a new form of cell death induced by iron-dependent lipid peroxidation, which can be rescued by ferroptosis-specific inhibitors, such as Fer-1; iron chelators, such as DFO; and other antioxidants [37,38]. Compared with apoptosis, this nonapoptotic cell death is characterized by various morphological features, such as an integrated cell membrane, a normal nuclear size without chromatin agglutination, and small mitochondria with thick mitochondrial membranes [37]. Ferroptosis is also accompanied by several biological features, including an accumulation of iron and ROS, and the dissipation of the mitochondrial membrane potential [37]. The consistency between our observations and most features of ferroptosis prompted us to further explore the protection of the Fer-1 ferroptosis-specific inhibitor and the DFO iron chelator. However, it should be mentioned that more indicators and cell species are required to sufficiently demonstrate whether the form of cell death observed in this study could be classified as ferroptosis or other nonapoptotic death. This will be explored further in our future work.

Clinically, the regulation of dyslipidemia, inhibition of high fatty acid metabolism in patients with diabetes, and application of β-adrenoceptor blockers might be potential therapeutic approaches for reducing SH-induced cardiovascular events. However, many obstacles remain before these approaches can reach practical application. For example, lipid-lowering therapy might affect blood glucose control and increase insulin resistance [39]. Sympathetic nerve activation exerts a defensive function, such as promoting an increase in the level of blood glucose and stimulating feeding behavior [40]. β-Adrenoceptor blockers might mask the vigilant state of hypoglycemia in diabetes, thereby increasing the incidence of SH [41]. Moreover, the timing of SH events are unpredictable; once they occur, self-protection is lost. Therefore, it might be more feasible to prevent hypoglycemia-induced cardiovascular disease by focusing on the risk factors in the diabetic stage. Considering the synergistic effect, exploring the mechanisms of the synergistic effect between high fatty acid metabolism and sympathetic activation might have potential significance for future treatments. In this study, we demonstrated that mtROS production during high fatty acid metabolism was the key to impairing cardiomyocyte resistance to β-adrenoceptor hyperactivation. However, whether there are more synergistic factors related to or irrelevant to mtROS between diabetes and hypoglycemia warrants further investigation.

6. Limitations

There were several limitations to the present study. First, whether the synergistic effect of high fatty acid metabolism and β-adrenoceptor activation exists in all types of cardiomyocytes remains to be elucidated. Second, the human body possesses an intricate system determining the differences in this synergism in in vivo and *in vitro* experiments. Third, the mechanism of cell death induced by this synergism and whether it widely exists in different types of cardiomyocytes under the same intervention needs further investigation.

In conclusion, our study revealed that high fatty acid metabolism attenuates cardiomyocyte resistance to β-adrenoceptor hyperactivation, partly explaining the differential outcome of the SH-induced cardiac function and myocardial energy metabolism in diabetic and nondiabetic mice. It was further confirmed that mtROS plays a key role in this synergistic effect, providing potential therapeutic targets for preventing adverse cardiac outcomes due to SH in diabetes. We speculated that this synergistic effect might also be the main effector of pathogenesis of other cardiovascular diseases, and further exploration of the specific mechanism in this interaction will be required in future work.

Sources of funding

The collection, analysis and interpretation of data in this study was supported by the Financial Department Special Funds of Fujian Province (2018B041), the Construction Program of Key Clinical Specialty of Fujian Province [(2015)593], the Startup Fund for Scientific Research of Fujian Medical University (2018QH2031), and the Joint Foundation Program of Innovation Project of Science and Technology of Fujian Province (2017Y9060).

Declaration of competing interest

None.

Acknowledgements

We acknowledge the Public Technology Service Center Fujian Medical University for providing technical support in laser confocal microscope. We would like to thank Editage for English language editing.

References

[1] Hypoglycaemia, cardiovascular disease, and mortality in diabetes: epidemiology, pathogenesis, and management, Lancet Diabetes Endocrinol. 7 (2019) 385–396.
[2] M. Hanefeld, B.M. Frier, F. Pistrosch, Hypoglycemia and cardiovascular risk: is there a major link? Diabetes Care 39 (Suppl 2) (2016) S205–S209.
[3] L. Huang, Y. Zhou, Z. Chen, M. Zhang, Z. Zhan, L. Wang, L. Liu, Severe hypoglycemia exacerbates myocardial dysfunction and metabolic remodeling in diabetic mice, Mol. Cell. Endocrinol. 503 (2020), 110692.
[4] C.V. Desouza, G.B. Bolli, V. Fonseca, Hypoglycemia, diabetes, and cardiovascular events, Diabetes Care 33 (2010) 1389–1394.
[5] C.M. Reno, D. Daphna-Iken, Y.S. Chen, J. VanderWeele, K. Jethi, S.J. Fisher, Severe hypoglycemia-induced lethal cardiac arrhythmias are mediated by sympathoadrenal activation, Diabetes 62 (2013) 3570–3581.
[6] Y. Shao, B. Redfors, M. Ståhlman, M.S. Täng, A. Miljanovic, H. Möllmann, C. Troidl, S. Szardien, C. Hamm, H. Nef, J. Borén, E. Omerovic, A mouse model reveals an important role for catecholamine-induced lipotoxicity in the pathogenesis of stress-induced cardiomyopathy, Eur. J. Heart Fail. 15 (2013).
[7] E. Chow, A. Bernjak, E. Walkinshaw, A. Lubina-Solomon, J. Freeman, I. A. Macdonald, P.J. Sheridan, S.R. Heller, Cardiac autonomic regulation and repolarization during acute experimental hypoglycemia in type 2 diabetes, Diabetes 66 (2017) 1322–1333.
[8] R.P. Hoffman, C.A. Sinkey, E.A. Anderson, Hypoglycemia increases muscle sympathetic nerve activity in IDDM and control subjects, Diabetes Care 17 (1994) 673–680.
[9] P.C. Schulze, K. Drosatos, I.J. Goldberg, Lipid use and misuse by the heart, Circ. Res. 118 (2016) 1736–1751.
[10] C.-R. Chong, K. Clarke, E. Levelt, Metabolic remodeling in diabetic cardiomyopathy, Cardiovasc. Res. 113 (2017) 422–430.
[11] K. Tsushima, H. Bugger, A.R. Wende, J. Soto, G.A. Jenson, A.R. Tor, R. McGlauflin, H.C. Kenny, Y. Zhang, R. Souvenir, X.X. Hu, C.L. Sloan, R.O. Pereira, V.A. Lira, K. W. Spitzer, T.L. Sharp, K.I. Shoghi, G.C. Sparagna, E.A. Rog-Zielinska, P. Kohl, O. Khalimonchuk, J.E. Schaffer, E.D. Abel, Mitochondrial reactive oxygen species in lipotoxic hearts induce post-translational modifications of AKAP121, DRP1, and OPA1 that promote mitochondrial fission, Circ. Res. 122 (2018) 58–73.
[12] A.W. Tank, D. Lee Wong, Peripheral and central effects of circulating catecholamines, Compr. Physiol. 5 (2015).
[13] S. Boudina, S. Sena, H. Theobald, X. Sheng, J.J. Wright, X.X. Hu, S. Aziz, J. I. Johnson, H. Bugger, V.G. Zaha, E.D. Abel, Mitochondrial energetics in the heart

in obesity-related diabetes: direct evidence for increased uncoupled respiration and activation of uncoupling proteins, Diabetes 56 (2007) 2457–2466.
[14] E.-M. Jeong, M. Liu, M. Sturdy, G. Gao, S.T. Varghese, A.A. Sovari, S.C. Dudley, Metabolic stress, reactive oxygen species, and arrhythmia, J. Mol. Cell. Cardiol. 52 (2012) 454–463.
[15] H. Xiao, H. Li, J.-J. Wang, J.-S. Zhang, J. Shen, X.-B. An, C.-C. Zhang, J.-M. Wu, Y. Song, X.-Y. Wang, H.-Y. Yu, X.-N. Deng, Z.-J. Li, M. Xu, Z.-Z. Lu, J. Du, W. Gao, A.-H. Zhang, Y. Feng, Y.-Y. Zhang, IL-18 cleavage triggers cardiac inflammation and fibrosis upon β-adrenergic insult, Eur. Heart J. 39 (2018) 60–69.
[16] W. Liu, A. Ruiz-Velasco, S. Wang, S. Khan, M. Zi, A. Jungmann, M. Dolores Camacho-Muñoz, J. Guo, G. Du, L. Xie, D. Oceandy, A. Nicolaou, G. Galli, O. J. Müller, E.J. Cartwright, Y. Ji, X. Wang, Metabolic stress-induced cardiomyopathy is caused by mitochondrial dysfunction due to attenuated Erk5 signaling, Nat. Commun. 8 (2017) 494.
[17] R. Ni, T. Cao, S. Xiong, J. Ma, G.-C. Fan, J.C. Lacefield, Y. Lu, S. Le Tissier, T. Peng, Therapeutic inhibition of mitochondrial reactive oxygen species with mito-TEMPO reduces diabetic cardiomyopathy, Free Radic. Biol. Med. 90 (2016) 12–23.
[18] T. Tien, J. Zhang, T. Muto, D. Kim, V.P. Sarthy, S. Roy, High glucose induces mitochondrial dysfunction in retinal müller cells: implications for diabetic retinopathy, Invest. Ophthalmol. Vis. Sci. 58 (2017) 2915–2921.
[19] M. Maus, M. Cuk, B. Patel, J. Lian, M. Ouimet, U. Kaufmann, J. Yang, R. Horvath, H.-T. Hornig-Do, Z.M. Chrzanowska-Lightowlers, K.J. Moore, A.M. Cuervo, S. Feske, Store-operated Ca entry controls induction of lipolysis and the transcriptional reprogramming to lipid metabolism, Cell Metabol. 25 (2017) 698–712.
[20] K. Fujiwara, H. Tanaka, H. Mani, T. Nakagami, T. Takamatsu, Burst emergence of intracellular Ca2+ waves evokes arrhythmogenic oscillatory depolarization via the Na+-Ca2+ exchanger: simultaneous confocal recording of membrane potential and intracellular Ca2+ in the heart, Circ. Res. 103 (2008) 509–518.
[21] R. Salie, J.A. Moolman, A. Lochner, The mechanism of beta-adrenergic preconditioning: roles for adenosine and ROS during triggering and mediation, Basic Res. Cardiol. 107 (2012) 281.
[22] J.Q. Kwong, J.D. Molkentin, Physiological and pathological roles of the mitochondrial permeability transition pore in the heart, Cell Metabol. 21 (2015) 206–214.
[23] A.P. Halestrap, What is the mitochondrial permeability transition pore? J. Mol. Cell. Cardiol. 46 (2009) 821–831.
[24] S.C. Kolwicz, S. Purohit, R. Tian, Cardiac metabolism and its interactions with contraction, growth, and survival of cardiomyocytes, Circ. Res. 113 (2013) 603–616.
[25] Hypoglycaemia, cardiovascular disease, and mortality in diabetes: epidemiology, pathogenesis, and management, Lancet Diabetes Endocrinol. 7 (2019) 385–396.
[26] D.D. Belke, T.S. Larsen, E.M. Gibbs, D.L. Severson, Altered metabolism causes cardiac dysfunction in perfused hearts from diabetic (db/db) mice, Am. J. Physiol. Endocrinol. Metab. 279 (2000) E1104–E1113.
[27] M.A. Alpert, K. Karthikeyan, O. Abdullah, R. Ghadban, Obesity and cardiac remodeling in adults: mechanisms and clinical implications, Prog. Cardiovasc. Dis. 61 (2018) 114–123.
[28] A. Thiele, K. Luettges, D. Ritter, N. Beyhoff, E. Smeir, J. Grune, J.S. Steinhoff, M. Schupp, R. Klopfleisch, M. Rothe, N. Wilck, H. Bartolomaeus, A.K. Migglautsch, R. Breinbauer, E.E. Kershaw, G.F. Grabner, R. Zechner, U. Kintscher, A. Foryst-Ludwig, Pharmacological inhibition of adipose tissue Adipose Triglyceride Lipase (ATGL) by Atglistatin prevents catecholamine-induced myocardial damage, Cardiovasc. Res. (2021), cvab182.
[29] J. Nunnari, A. Suomalainen, Mitochondria: in sickness and in health, Cell 148 (2012) 1145–1159.
[30] G. Benard, R. Rossignol, Ultrastructure of the mitochondrion and its bearing on function and bioenergetics, Antioxidants Redox Signal. 10 (2008) 1313–1342.
[31] M.D. Brand, D.G. Nicholls, Assessing mitochondrial dysfunction in cells, Biochem. J. 435 (2011) 297–312.
[32] A. Riojas-Hernández, J. Bernal-Ramírez, D. Rodríguez-Mier, F.E. Morales-Marroquín, E.M. Domínguez-Barragán, C. Borja-Villa, I. Rivera-Álvarez, G. García-Rivas, J. Altamirano, N. García, Enhanced oxidative stress sensitizes the mitochondrial permeability transition pore to opening in heart from Zucker Fa/fa rats with type 2 diabetes, Life Sci. 141 (2015) 32–43.
[33] P. Pérez-Treviño, J. Sepúlveda-Leal, J. Altamirano, Simultaneous assessment of calcium handling and contractility dynamics in isolated ventricular myocytes of a rat model of post-acute isoproterenol-induced cardiomyopathy, Cell Calcium 86 (2020), 102138.
[34] D.W. Ito, K.I. Hannigan, D. Ghosh, B. Xu, S.G. Del Villar, Y.K. Xiang, E.J. Dickson, M.F. Navedo, R.E. Dixon, β-adrenergic-mediated dynamic augmentation of sarcolemmal Ca 1.2 clustering and co-operativity in ventricular myocytes, J. Physiol. 597 (2019) 2139–2162.
[35] D. Hausenloy, A. Wynne, M. Duchen, D. Yellon, Transient mitochondrial permeability transition pore opening mediates preconditioning-induced protection, Circulation 109 (2004) 1714–1717.
[36] G. Kroemer, L. Galluzzi, C. Brenner, Mitochondrial membrane permeabilization in cell death, Physiol. Rev. 87 (2007).
[37] Y. Xie, W. Hou, X. Song, Y. Yu, J. Huang, X. Sun, R. Kang, D. Tang, Ferroptosis: process and function, Cell Death Differ. 23 (2016) 369–379.
[38] S.J. Dixon, K.M. Lemberg, M.R. Lamprecht, R. Skouta, E.M. Zaitsev, C.E. Gleason, D.N. Patel, A.J. Bauer, A.M. Cantley, W.S. Yang, B. Morrison, B.R. Stockwell, Ferroptosis: an iron-dependent form of nonapoptotic cell death, Cell 149 (2012) 1060–1072.
[39] B. Zafrir, M. Jain, Lipid-lowering therapies, glucose control and incident diabetes: evidence, mechanisms and clinical implications, Cardiovasc. Drugs Ther. 28 (2014) 361–377.
[40] A. Iqbal, S. Heller, Managing hypoglycaemia, Best Pract. Res. Clin. Endocrinol. Metabol. 30 (2016) 413–430.
[41] D.A. Popp, T.F. Tse, S.D. Shah, W.E. Clutter, P.E. Cryer, Oral propranolol and metoprolol both impair glucose recovery from insulin-induced hypoglycemia in insulin-dependent diabetes mellitus, Diabetes Care 7 (1984) 243–247.